Island wakes in the Southern California Bight

R. M. A. Caldeira,[1,2] P. Marchesiello,[3] N. P. Nezlin,[4] P. M. DiGiacomo,[5] and J. C. McWilliams[3]

Received 19 August 2004; revised 21 February 2005; accepted 14 June 2005; published 18 November 2005.

[1] Wind- and current-induced island wakes were investigated using a multiplatform approach of in situ, remote sensing, and numerical model simulations for the Southern California Bight (SCB). Island wind wakes are a result of sheltering from the wind, with weak wind mixing, strong heat storage, and consequent high sea surface temperature (SST). Wind wakes around Santa Catalina Island are most persistent during spring and summer months. Current wakes, caused by the disruption of the poleward traveling California Countercurrent, induce eddies to form off the north end of Catalina Island, and these move poleward every 9–12 days. Current wake eddies induce strong mixing, with low SST and high-density sea surface signatures, whereas wind wakes induce high sea surface temperature signatures associated with the formation of a well-defined shallow thermocline. Current wake eddies vary from 1 to 30 km in diameter. From numerical solutions we predicted the frequency of occurrence of current-induced wakes off Santa Catalina Island. Wind wakes were also observed off all the other islands of the SCB as seen from the analysis of synthetic aperture radar data. Time series analysis of the island mass effect phenomenon has shown a concurrence of low SST and high sea surface chlorophyll for Santa Catalina, San Nicholas, and San Clemente islands that might be related to the seasonality of the California Current and California Countercurrent. Future oceanographic research in the SCB should not ignore the occurrence of wind- and current-induced island features since they may be important in the transport and/or retention of nutrients, pollutants, and plankton.

Citation: Caldeira, R. M. A., P. Marchesiello, N. P. Nezlin, P. M. DiGiacomo, and J. C. McWilliams (2005), Island wakes in the Southern California Bight, *J. Geophys. Res.*, *110*, C11012, doi:10.1029/2004JC002675.

1. Introduction

[2] Island wakes have been intensively studied. The term has been used to refer to wind-induced wakes formed on the leeward side of islands because of the sheltering from the wind with concomitant weaker mixing, and warm sea surface temperatures. Current wakes are formed when bathymetry deflects incoming ocean currents with eddy formation and upwelling of cool deep water often associated with high productivity. It is important that wind wakes on the sea surface not be confused with atmospheric wind wakes on the lee of an island, such as atmospheric Von Karman Vortex Streets [see, e.g., *Caldeira et al.*, 2002]. We use the term wind wakes here to refer to the effect of the wind on sea surface thermal patterns caused by the sheltering from the island's orography.

[3] Island wakes are also related to the "island mass effect." The island mass effect concept was first described by *Doty and Oguri* [1956] as an increase in "biological productivity," that is, chlorophyll concentration, on the east side of Oahu Island in the Hawaiian Archipelago. Subsequently, the effect of island bathymetry on ambient oceanography was generalized to include island effects around entire islands [*Hamner and Hauri*, 1981a], and island mass effects now include differences in phytoplankton, zooplankton and fish biomass due to the formation of island-induced wakes, eddies, fronts, filaments and upwelling processes [see also *Aristegui et al.*, 1994, 1997; *Hernandez-Leon*, 1988, 1991; *Rissik et al.*, 1997].

[4] *Owen* [1980] first identified eddy-like motions offshore of Santa Catalina Island. Sea surface drogue trajectories showed trapping and circular motions to the southeast side of Santa Catalina Island, but no mention was made of the formation of a possible current wake. In fact, most oceanographic characterizations of the Southern California Bight (SCB) thereafter have not been concerned with the small-scale circulation around the islands [*Bray et al.*, 1999; *Hickey*, 1979, 1991, 1992, 1993, 1998]. Most recently [*DiGiacomo and Holt*, 2001], have described an abundance of small-scale eddies (less than 50 km) occurring

[1]Los Angeles Marine Science Center, University of California, Los Angeles, California, USA.
[2]Now at Center for Macaronesian Studies, University of Madeira, Madeira Island, Portugal.
[3]Institute of Geophysics and Planetary Physics, University of California, Los Angeles, California, USA.
[4]Southern California Coastal Water Research Project, Westminster, California, USA.
[5]Jet Propulsion Laboratory, California Institute of Technology, Pasadena, California, USA.

0148-0227/05/2004JC002675$09.00

in the San Pedro, Santa Catalina and Santa Barbara Basins induced by the island and coastline bathymetry.

[5] Studies on both wind- and current-induced island wakes have been carried out around the Canary Island Archipelago [*Aristegui et al.*, 1994, 1997; *Barton et al.*, 1998, 2000]. *Barton et al.* [2000] clearly distinguished cyclonic and anticylonic current eddies downstream of Gran Canaria (Canary Islands), from warm surface wind–induced wakes leeward of the island using sea surface temperature (SST) from satellite images.

[6] Our study in the Southern California Bight investigates the differences between island wakes induced by the wind, and island wakes induced by ocean currents flowing past the island's shelf. It is an expansion on the brief discussion of these issues presented by *Caldeira and Marchesiello* [2002]. It is also an attempt to characterize the biological consequences of these wakes, the so-called "island mass effect." We also focus on the historically overlooked discussion on submesoscale circulation patterns (<10 km) around the SCB. First, we start by setting the historical oceanographic scenarios for the region. Second, we use a case study around Santa Catalina Island to distinguish between wind- and current-induced island wakes, using in situ, remote sensing and numerical modeling data. Third, we expand our description of island wakes to include observations on other islands of the Southern California Bight. Last, we attempt to quantify the "island mass effect" using a time series analysis from Sea-viewing Wide Field-of-view Sensor (SeaWiFS) derived sea surface chlorophyll and Advanced Very High Resolution Radiometer (AVHRR)-SST data.

2. Geographic Setting

[7] South of Point Conception (PC) the coastline forms a basin called the Southern California Bight (SCB)(Figure 1). The SCB consists of a set of basins separated by islands and underwater ridges. It is bordered by a narrow shelf 3 to 6 km wide, mostly shallower than 50 m. The basins between ridges are rather deep (>500 m). The stream of the California Current (CC) turns to south-southeast and passes along the continental slope. At about 32°N a branch of the California Current turns eastward and then northward along the coast of the Southern California Bight, forming a large gyre known as the Southern California Eddy (SCE). The poleward travelling current along the coast is known as the California Countercurrent (CCC) and transports warm water (often poor in chlorophyll) into the Santa Monica Basin and the Santa Barbara Channel. At the northwestern end of Santa Monica Basin, the poleward flow divides into two flows: one flowing northwestward through the Santa Barbara Channel, and the other flowing westward to the south of the Channel Islands [*Sverdrup and Fleming*, 1941; *Lynn and Simpson*, 1987; *Hickey*, 1992; *Bray et al.*, 1999].

[8] The intensity of the California Current System varies seasonally. During winter and summer the poleward transport of the California Countercurrent intensifies and the jet of the California Current migrates offshore, while warm southern waters penetrate further to the north and west within the Southern California Bight [*Reid and Mantyla*, 1976; *Hickey*, 1979; *Bray et al.*, 1999; *Haney et al.*, 2001].

[9] The strongest equatorward winds occur during spring along most of the California Coast [*Hickey*, 1998]. Also during spring the CC is closer to shore and becomes increasingly jet-like, with predominantly equatorward flow in the SCB. Winds in the SCB are generally weaker than north of Point Conception, with significant daily and seasonal fluctuations. In general, the correspondence between ocean current transport and wind stress and/or curl is not particularly good for the SCB. One exception, however, is that in spring, equatorward anomalies in ocean current transport near the coast are associated with equatorward wind stress anomalies as would be expected from coastal upwelling. Another correspondence is that positive curl in the average wind fields, inshore of about 200 km, is associated with poleward ocean flow. Northwesterly wind dominates all year round (offshore). During winter the wind direction is more variable; from March to November northwesterly wind is steadier. Maximum wind speed is observed in spring decreasing during summer months [*Bray et al.*, 1999].

[10] Santa Catalina Island is located in the SCB at 33.3°N 118.3°W. The island is 33.7 km long by 11.7 km at its widest part. The island stands on its own shelf, 32km offshore from the Palos Verdes Peninsula and 31 km from San Clemente Island (Figure 1). The San Pedro Basin between Catalina and the mainland reaches depths of 880 m. The Catalina Basin, between Santa Catalina and San Clemente Island, reaches depths of 1200 m. Catalina Island has a ridge of mountains extending from northwest to southeast, seen in the synthetic aperture radar (SAR) image (Figure 2a), that can reach 640 m above sea level.

[11] An ERS-1 SAR image acquired 28 May 2004 illustrates some of the submesoscale complexity in the Santa Catalina Island and San Pedro Basin region. A current wake with spiral eddies was detected to the northwest of Santa Catalina Island whereas to the east, sheltered from the mountain range, there was a wind-induced wake forming (see dark patch of reduced backscatter in Figure 2a). AVHRR data from the next day clearly showed the sea surface signature of warm water in the wind wake region (21°C), whereas north of the island the waters at the surface were 18°C (Figure 2b).

3. Data and Methods

3.1. SAR Data

[12] SAR imagery provides fine-resolution active microwave observations of sea surface roughness not affected by cloud cover or availability of light. Factors modulating sea surface roughness include wind, interactions of waves and currents, and the presence of oils and surfactants on the ocean surface. Variability in observed surface roughness ($\sim$ backscatter) can be used to visualize numerous dynamic oceanographic and boundary layer features, for example, fronts and eddies [*Munk et al.*, 2000; *DiGiacomo and Holt*, 2001] atmospheric waves and wind shadowing [*Clemente-Colon and Yan*, 2000] and pollution hazards [*DiGiacomo et al.*, 2004]. The ERS-1 and ERS-2 (hereafter ERS-1/2) SAR data utilized in this study were obtained from the European Space Agency (ESA); images were acquired at the receiving station operated by the Canada Centre of Remote Sensing in Prince Albert, Saskatchewan. The Canadian Space Agency's RADARSAT SAR data used here were received by the same Prince Albert receiving station and processed at the Alaska Satellite Facility,

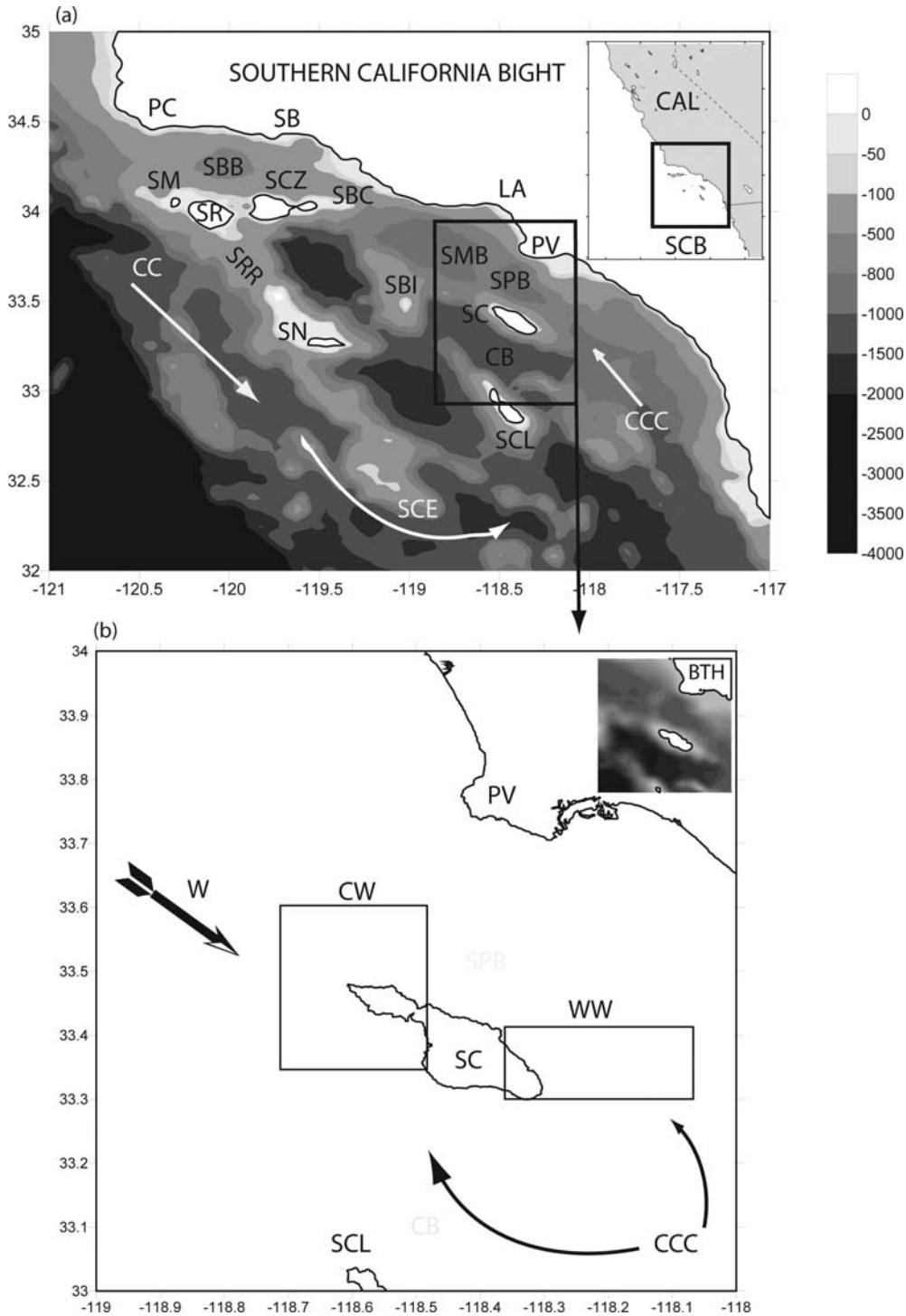

Figure 1. (a) Southern California Bight (SCB) map showing the different locations mentioned in the text: CAL, California; PC, Point Conception; SB, Santa Barbara; LA, Los Angeles; PV, Palos Verdes Peninsula; SM, San Miguel Island; SR, Santa Rosa Island; SRR, Santa Rosa Ridge; SCZ, Santa Cruz Island; SBB, Santa Barbara Basin; SBC, Santa Barbara Channel; SBI, Santa Barbara Island; SN, San Nicolas Island; SMB, Santa Monica Basin; SPB, San Pedro Basin; SC, Santa Calatina Island; CB, Catalina Basin; SCL, San Clemente Island; CC, California Current; SCE, Southern California Eddy; and CCC, California Countercurrent. (b) Proposed hypothesis: California Countercurrent reaches Santa Catalina Island, forming a current-induced wake (CW) to the north; opposite wind (W) causes a wind-induced wake (WW) leeward of Catalina (to the southeast). A detail of the bathymetry (BTH) is shown for the same region.

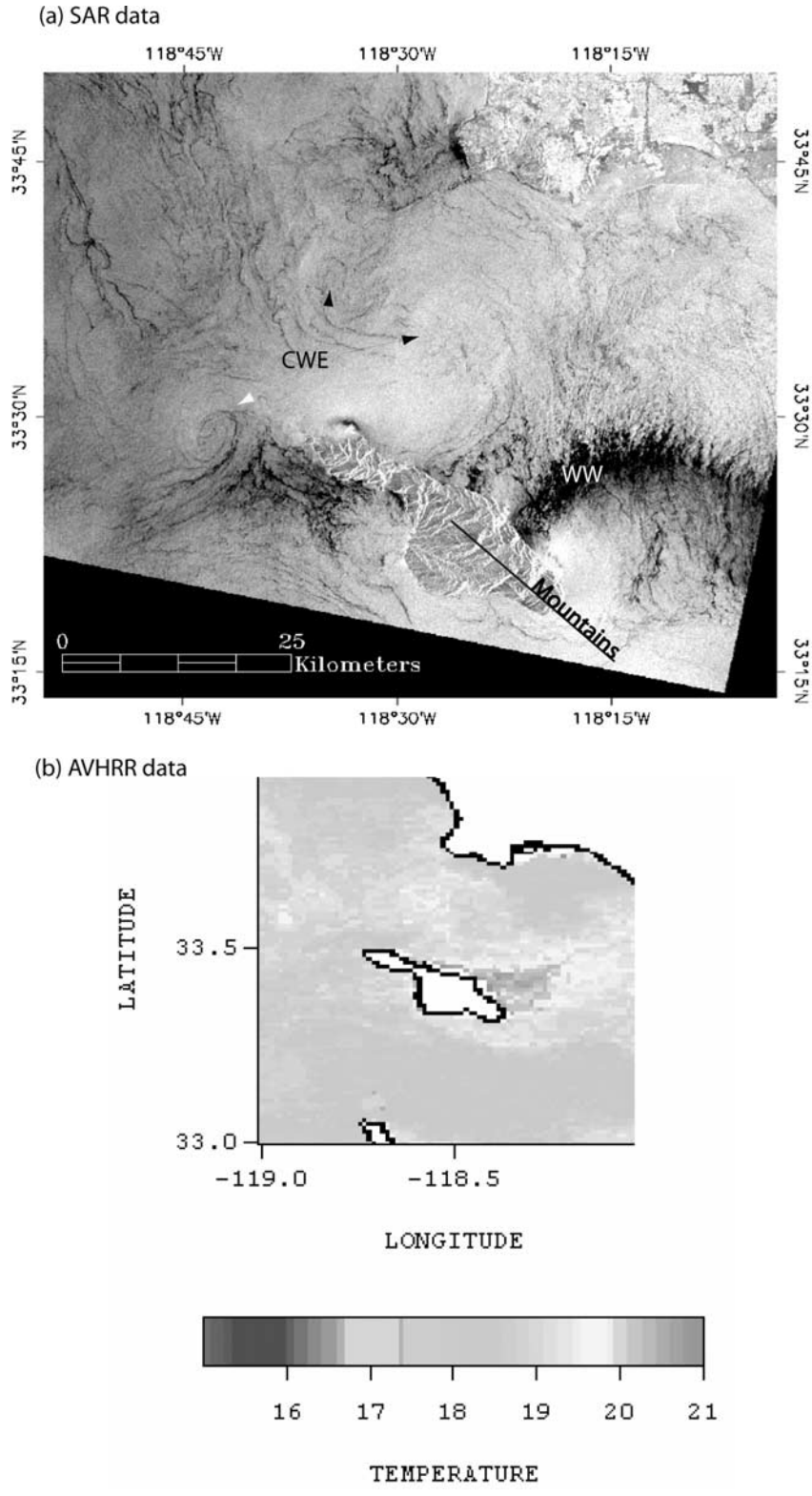

Figure 2. (a) ERS-1 synthetic aperture radar (SAR) image acquired 28 May 1994 at 1834 UTC. Spiral current wake eddies (~10 km in diameter) are visible off the northwest end of Santa Catalina Island (CWE), as is a wind wake (WW) off the island's eastern end. Other features are visible in the channel adjoining the mainland. Copyright ESA 1994. (b) AVHRR data collected on 29 May (0038 UTC). A warm wind–induced wake is visible in the lee of Catalina. See color version of this figure at back of this issue.

located at the University of Alaska in Fairbanks, Alaska. RADARSAT data were also acquired via an onboard tape recorder. The ERS-1/2 and RADARSAT SAR instruments all operate at a C band frequency of 5.3 GHz, but differ in their polarizations: vertical transmit–vertical receive (VV) for ERS-1/2; horizontal transmit–horizontal receive (HH) for RADARSAT. Data were obtained in one of two configuration modes: (1) standard beam mode for both ERS-1/2 and RADARSAT which has a swath width of 100 km, a pixel size of 12.5 m (averaged to 100 m here), and operates over varying fixed ranges of incidence angles and (2) for RADARSAT only, the ScanSAR wide-beam B mode, which has a swath width of 450 km over incidence angles from 20° to 47° and a 100 m pixel size in the imagery presented here.

3.2. AVHRR SST Data

[13] The daily satellite images of sea surface temperature (SST) were obtained from the CoastWatch program. SST was measured by Advanced Very High Resolution Radiometers (AVHRR) on the National Oceanic and Atmospheric Administration (NOAA) series polar-orbiting meteorological satellites. The AVHRR sensor measures radiance from the ocean surface in five near-infrared and infrared channels with 1.1-km spatial resolution at nadir. Satellite images were processed at NOAA CoastWatch data center. SST estimates were made by converting the radiance measured in the infrared channels to brightness temperature and then using a multichannel technique [*McClain et al.*, 1985] to calculate SST to within ±0.5°C. Cloud identification masks were created using visible and infrared channels with a series of spectral gradient, difference, and threshold tests.

3.3. Wind Data

[14] The wind data were obtained from the Coupled Ocean/Atmosphere Mesoscale Prediction System (COAMPS) from the Naval Research Laboratory (NRL). COAMPS uses a 9 km mesh grid in the SCB nested within 27 km grid spacing. COAMPS includes automated complex quality control software, a multivariate optimum interpolation atmospheric analysis, and the COAMPS Ocean Data Assimilation System. The NRL Coupled Ocean/Atmosphere Mesoscale Prediction System–On Scene (COAMPS-OS) is an automated, portable, atmospheric nowcast/forecast data assimilation system. COAMPS-OS allows to independently assimilate local observations, satellite-derived observations and boundary conditions for a regional center and to maintain data assimilation, now cast, and a forecast capability. In order to study seasonal wind variability the data were averaged for each month of the year, from 1 October 1998 to 30 September 2000, so that persistent wind patterns would be revealed. Wind stress ($\tau = \rho_a C_D W^2$) was plotted overlaying gradients of calculated Ekman depths ($D_E = 0.7u^*/f$), where u^* is the friction velocity proportional to the wind, f is the Coriolis parameter, ρ_a is the density of air; C_D is the nondimensional drag coefficient ($\sim 1.4 \times 10^{-3}$) and W is the wind speed in ms^{-1}.

3.4. In Situ Data

[15] In situ data were acquired aboard UCLA's Marine Science center R/V Sea World UCLA. Thirty-two stations were visited in a grid distributed around Santa Catalina Island (see Figure 3a for station locations). At each station measurements of position, water visibility, wind speed and direction were taken. Conductivity-temperature-depth (CTD) casts and plankton samples were simultaneously collected at each station. CTD data were processed according to routines described by *Joint Panel on Oceanographic Tables and Standards* [1991]. Salinity and density was calculated on the basis of the equation of state for seawater (EOS80), with $\sigma_t = \rho(s, t, 0) - 1000$ kg m^{-3}).

3.5. Numerical Model Simulations

[16] Regional Ocean Modeling System (ROMS) is a free-surface, primitive equation, curvilinear coordinate oceanic model in which barotropic and baroclinic momentum equations are resolved separately. The model is written for multithreaded computer architectures and features high-order numerical schemes for space and time differencing, to optimize the effective resolution of the model. In addition, open boundary conditions in ROMS permit well-behaved, long-term solutions for coastal configurations with open boundaries on three sides, through which the influences of the large-scale, external circulation must be conveyed. Detailed description and validation of the model for the U.S. West coast is given by *Shchepetkin and McWilliams* [1998, 2003], *Marchesiello et al.* [2003], and *Shchepetkin and McWilliams* [2005].

[17] The local, small-scale dynamics in the SCB is studied using embedded domains. The method for embedded gridding takes advantage of the Adaptive Grid Refinement in FORTRAN (AGRIF) package [*Blayo and Debreu*, 1999], which has the ability to manage an arbitrary number of embedded levels. ROMS nesting procedure is described and validated for the USWC [*Penven et al.*, 2003]. Three levels of resolution have been defined: the first level is a 20-km grid USWC domain (forced at the open boundaries by Levitus data, using mixed active-passive boundary conditions as given by *Marchesiello et al.* [2001]; parent of a second level which is a 6-km grid subdomain of the whole SCB, which in turn is the parent of the third level, a 2-km grid subdomain of Santa Monica Basin (SMB) including Santa Catalina and San Clemente Islands.

[18] Using as forcing a monthly climatology extracted from COAMPS wind data, we have done a multiyear simulation in one-way nesting mode until the solution reached equilibrium. The solution for 1 year is qualitatively very comparable at the different levels, but the magnitudes of the current increases with finer resolutions. Moreover, the finest level shows small-scale processes not present in the parent levels.

[19] ROMS solutions are used to illustrate the diversity of currents wake scenarios that might occur around Santa Catalina Island. Seasonal means of sea surface height (SSH) are also calculated to help the discussion on seasonality of oceanic conditions around the island.

3.6. Time Series Analysis of Low-Resolution AVHRR-SST and SeaWiFS Chlorophyll Data

[20] The persistent signatures of these island wakes was analyzed using remote sensing data. Pathfinder data was used to quantify temporal differences in SST; the data was processed within the scope of NOAA/NASA AVHRR

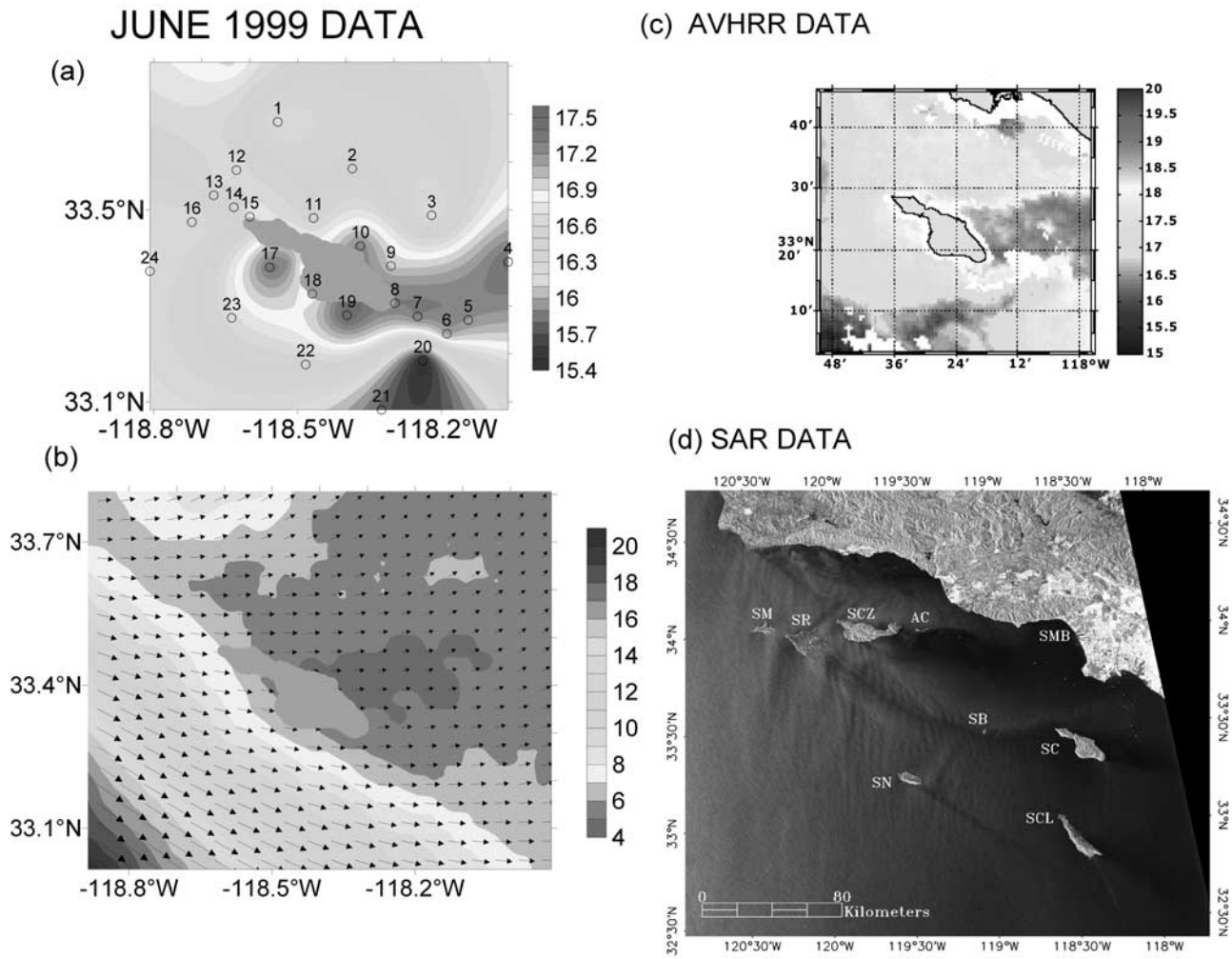

Figure 3. In situ data for June 1999: (a) temperature, (b) Ekman depths (D_E) and wind fields from COAMPS, (c) AVHRR data for the same period showing warmer SST leeward of Santa Catalina Island, and (d) RADARSAT ScanSAR image from 8 June 1999 at 0200 UTC of the entire Southern California Bight. Evident are the recurring wind wakes off the larger islands within the SCB. The Santa Rosa Island (SR) wind wake on this occasion appeared to reach all the way to Santa Catalina Island (SC). The Santa Cruz Island (SCZ) wind wake reached Santa Monica Bay (SMB). The San Nicholas (SN) wind wake runs (~50 km) to the southeast. Santa Catalina and San Clemente Island (SCL) wind wakes were also clearly visible. SM denotes San Miguel Island; AC denotes Ana Capa Island; and SB denotes Santa Barbara Island. Copyright Canadian Space Agency 1999. See color version of this figure at back of this issue.

Oceans Pathfinder Project at JPL. The sea surface temperature (SST) data were derived from AVHRR, using an enhanced nonlinear algorithm [*Walton*, 1988]. We used daily data for the descending pass (nighttime) on global equal-angle grids of 4096 pixels/360° (~9.28 km resolution). Only the "best SST" data (i.e., highest quality pixel values) were considered. The interim versions V4.1 (2000–2001) and V4.1 (1997–1999) were used to derive absolute SST values for the time series analysis.

[21] The remote-sensed data collected by SeaWiFS used in this study were obtained from NASA Goddard Space Flight Center Distributive Active Archive Center (GSFC DAAC) [*Acker et al.*, 2002]. The data allowed for the time series analysis of sea surface chlorophyll concentration from different sides and at different distances from the islands; we used daily level 3 standard mapped images (SMI) data of SeaWiFS surface chlorophyll calculated during reprocessing 4 (Version 4). Level 3 SMI SeaWiFS chlorophyll data are interpolated to a regular grid of equidistant cylindrical projection of 360°/4096 pixels (about 9.28 km) resolution (similar to Pathfinder SST). We understand that the values of sea surface chlorophyll concentration derived from satellite measurements are subject to significant inaccuracy due to technical problems with remote-sensed observations, therefore we do not attempt to compare the remote-sensed data to in situ chlorophyll absolute values. Rather, we use the remote-sensed observations for qualitative analysis of the cycles of phytoplankton development around the islands. Accordingly, we use the terms "remote-sensed surface chlorophyll concentration," "chlorophyll biomass" and "phytoplankton biomass" as synonyms, taking into account the correlation between remotely sensed surface pigment concentration and total pigment concentration in water column [*Smith and Baker*, 1978] and the good

correlation between satellite and in situ chlorophyll observations off California [*Chavez*, 1995].

[22] We calculated mean values within the grids of different size "quadrants" centered on each island. The smallest quadrants were 2 × 2 pixels, that is, about 19 × 19 km, for San Nicolas and San Clemente; for Santa Catalina, due to its shape and orientation within the SCB, the size the quadrants was 3 (horizontal) by 2 (vertical) pixels. Then mean chlorophyll values were estimated for quadrants of 4 × 4, 6 × 6, and 8 × 8 pixels (for Santa Catalina 4 × 6, 6 × 8, and 8 × 10, pixels respectively). The largest quadrant for each island was treated as the "background" chlorophyll concentration in the waters surrounding the island; the change in ratio between chlorophyll concentration in smaller quadrants and the background concentration (largest quadrant covering the whole island) was analyzed as a measure of the "island mass effect." For instance, if averaged monthly values for a particular quadrat were bellow 0, the quadrat was consistently colder or less productive than its regional counterpart; whereas if monthly values were above 0, the quadrat was warmer or more productive than its regional counterpart. We have also used the averaged monthly data from the regional quadrants to determine the seasonality of productivity around the islands.

4. Results and Discussion

4.1. Wind-Induced Wake

[23] We have assembled for the 11–13 June, 1999 cruise a mosaic of coincidental data collected in situ and from AVHRR and SAR satellite sensors (Figures 3a–3d). Surface temperature as measured by the CTD (Figure 3a) showed higher gradients mostly to the southeast of Catalina Island with temperatures varying from 17.2 to 17.5°C. This was also apparent in the wind and Ekman depth (D_E) patterns (Figure 3b). Winds were generally weaker leeward of the island than they were windward, hence the calculated D_E varied between 4m within the sheltered (leeward) region to up to 20m on the exposed (windward) region. Satellite AVHRR data for 13 June 1999 (2256 GMT), also showed a patch of warm SST leeward of Catalina Island (Figure 3c). Temperature in the warm patch varied between 18.5 to 20°C, whereas in the other areas sea surface temperatures only reached a maximum of 17°C. Differences between in situ and satellite SST values can be due to the fact that our in situ measurements were collected over a 3-day period (from 11–13 June 1999), whereas satellite data is a single observation in space and time. Furthermore, multichannel sea surface temperature (MCSST) algorithms also suffer from unaccounted processing inaccuracies [*Robinson*, 1997]. In any case, SST gradients for both platforms (in situ and remote sensing) show similar patterns, with warm water to the south of Catalina Island representative of the wind leeward wake. On 8 June 1999, RADARSAT ScanSAR imagery shows that there was a strong wind wake southeast of Catalina as revealed by a dark patch (i.e., zone of low backscatter) indicative of reduced sea surface roughness. In fact, this image reveals wind wakes had formed leeward of most of the islands in the SCB. The low-backscatter signal from the SAR image extends to 50 km offshore of Catalina Island and ~100 km offshore of Santa Cruz Island, sheltering part of the Santa Monica Bay (Figure 3d). Also readily apparent in this image are the concurrent sea surface manifestations of atmospheric lee waves, particularly southeast of Santa Rosa Island.

[24] As previously proposed by *Caldeira and Marchesiello* [2002], these inshore sea surface warm signatures are probably a result of solar heating and weaker winds in SCB. Heat advection from southern tropical waters is the traditional explanation for high SST often observed in inshore regions of the SCB [*Hickey*, 1979]. Nevertheless, solar heating and weaker winds may also play an important role in the buildup of these lateral (inshore-offshore) SST gradients for the whole Bight [*Caldeira and Marchesiello*, 2002].

[25] In order to analyze the vertical structure of wind-induced wakes we selected CTD stations from our June 1999 cruise from exposed and sheltered regions around Santa Catalina Island. There are three types of thermoclines: permanent, seasonal and shallow thermoclines (Figure 4). It is evident that shallow thermoclines had a deeper signature (4 m) at the sheltered stations (stations 4, 5, 6, and 10) than at the exposed stations (2 m) (stations 16, 17, 23, and 24).

[26] Shallow thermoclines can be considered analogous to the previously defined "atmospheric mixed layers" [*Imberger*, 1985]. Calm conditions, often felt in the morning, can lead to daily heating of the surface layer. Afternoon sea breezes can deepen the surface layer and night cooling can removed heat accumulation. This should be a theme for further investigation in the SCB. Time series analysis of diurnal thermoclines could give us further insights on the mechanisms that contribute to warming and cooling of the inshore surface waters.

[27] Daytime heating in the absence of strong wind mixing, for the Canaries Archipelago also led to the formation of a warm, stratified layer at the surface. In exposed regions, strong wind-induced mixing masks the effect of surface heating to produce a uniform surface layer [*Barton et al.*, 1998]. The crucial difference here is that these wind wake effects for Catalina Island seem to be associated with gradients in much shallower water (2–4 m); whereas in the Canaries these wind wakes were attributed to wind curl effects with much deeper signatures.

[28] In order to evaluate the daily persistence of this wind-induced wake event, around Santa Catalina Island, we have taken 2-year (1998–2000) wind (COAMPS) and AVHRR SST data sets and calculated monthly averages (Figure 5). We elected to present only the three representative (spring and summer) months out of the twelve month series because that is when the wind wakes were most prominent. The results, shown in Figure 5, revealed that the wind-induced wake signature is present during both spring and summer months sampled. Wind stress was weaker and Ekman depths were shallower (25–27 m) leeward of the island. Concurrently, warmer SST was also observed (17°C–20°C) leeward of the island.

[29] In their review of small-scale eddies of the SCB using SAR and AVHRR data [*DiGiacomo and Holt*, 2001] has also detected features with warm and cold surface signatures between the southeast side of Catalina Island and the coast (Palos Verdes Peninsula). Prior to that, *Owen* [1980] reported eddy-like patterns in drogue tracks on the wind wake side of Catalina Island. The contribution of

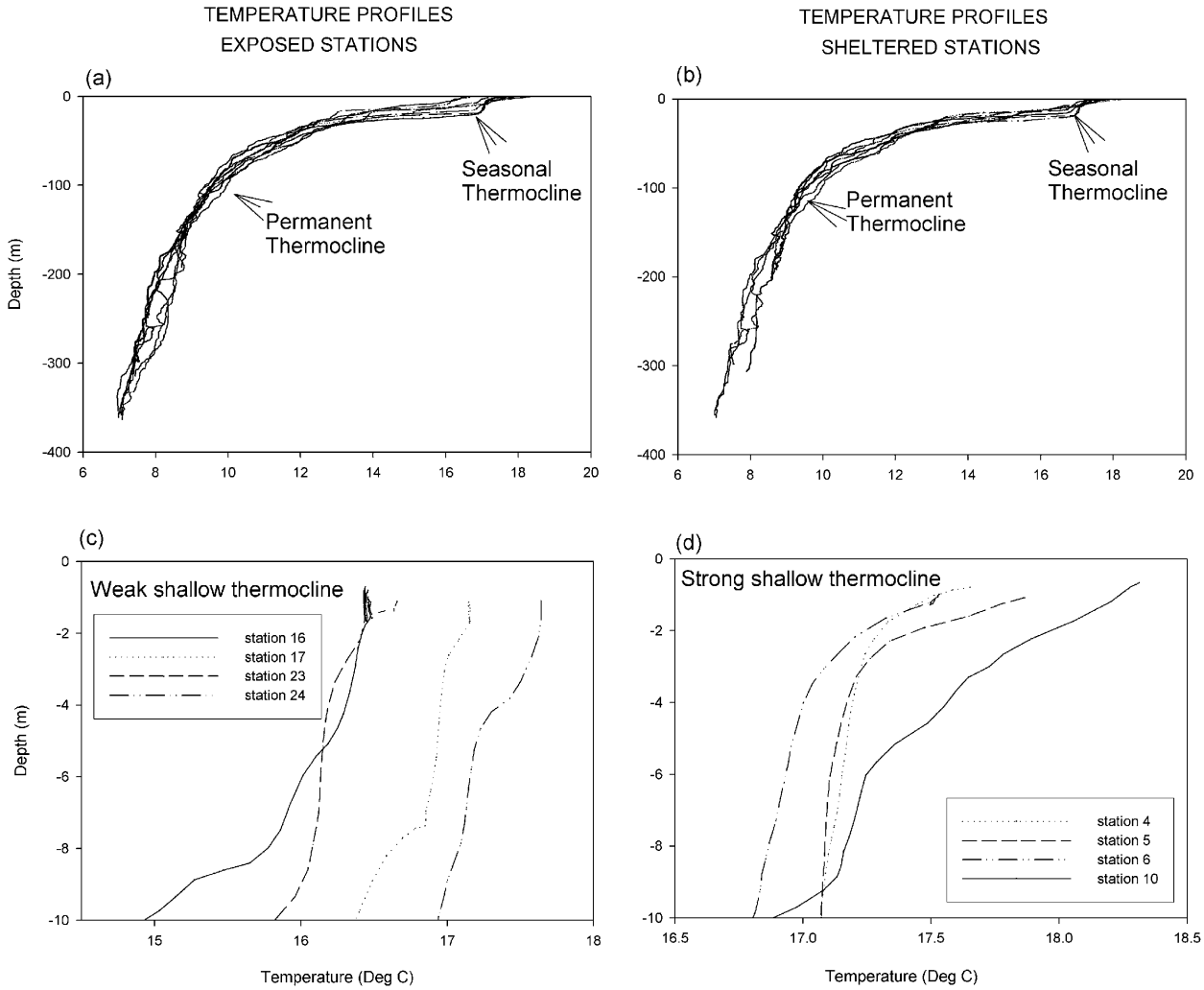

Figure 4. Temperature profiles in (a and c) exposed and (b and d) sheltered stations. The plots represent different scales of depth and temperature in order to emphasize the different-scale thermal gradients, that is, shallow, seasonal, and permanent thermoclines. Stations 4, 5, 6, and 10 (see Figure 3 for station locations) were on the leeward (sheltered) side of Santa Catalina Island, whereas stations 16, 17, 23, and 24 were on the windward (exposed) side. A better defined shallow thermocline is observed in the sheltered stations compared with weak shallow stratification on the exposed stations.

wind-induced eddies to the production of both cyclonic and anticyclonic eddies requires further investigation in SCB before conclusions can be drawn.

4.2. Current-Induced Wake

4.2.1. In Situ Data

[30] A mosaic data from the 16–20 November 2001 cruise reveals a nucleus of cold water (17.4°C) at the surface, northwest of Catalina Island (Figure 6a). High-density water (24.36 kg m^{-3}) was also detected in the same general area (Figure 6c). Coincidental SST from AVHRR (19 November 2001) showed a tongue of 17°C in the same region (Figure 6d). A RADARSAT SAR image (Figure 6e) acquired within this same period of time (i.e., 16 November 2001) indicates the presence of an eddy feature, to the northwest of Catalina. Other features were present off the southeast end of the island, including a low-wind zone and more surface slicks.

4.2.2. Reynolds Number Theory

[31] Current-induced island wakes is a classic fluid dynamics problem [*Barkley*, 1972; *Coutis and Middleton*, 1999; *Dietrich et al.*, 1996; *Furukawa and Wolanski*, 1998; *Wolanski et al.*, 1984, 1996]. The simplest two-dimensional approach, considering incident laminar flow, is to predict the formation of wake types, that is, from attached eddies to fully turbulent Von Karman Vortex Streets, on the basis of the Reynolds number (R_e) theory: $R_e = UL/A_h$, where U is the incident current speed; L the width of the island and A_h the horizontal Austauch coefficient, which is a measure of the horizontal eddy diffusivity. At very low R_e ($R_e < 0.5$), flow around obstacles is controlled by friction occurring entirely within the frictional boundary layer, and it is laminar and symmetric. At slightly larger Reynolds numbers ($2 < R_e < 30$) the boundary layer separates behind the obstacle, creating a vortex pair with opposite rotation and central return flow. Moderately high R_e ($40 < R_e < 70$) leads

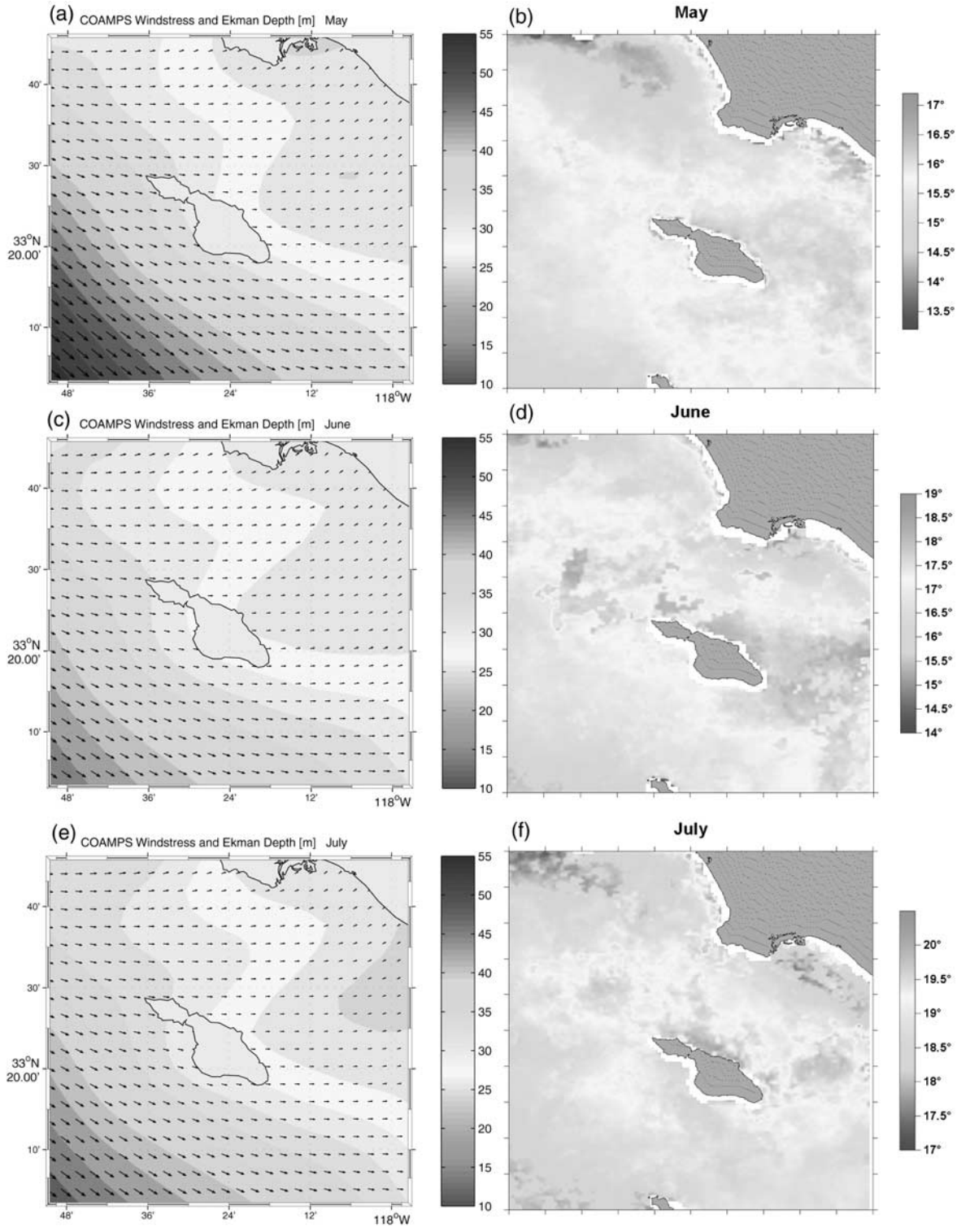

Figure 5. Average wind and SST conditions for the period of May to July (1998–2000 data). Left plots represent wind conditions and Ekman depths (D_E), color scale in meters, and right plots represent SST, color scale in degrees Celsius. As is evident, wind-sheltering effects off the southeast end of Santa Catalina occur most strongly during spring and summer. Winds are also generally stronger during spring and summer. Stronger winds caused stronger gradients on the Ekman depth, suggesting weaker wind mixing. Weaker mixing allows for higher heat storage and warmth of the SST leeward of the island (left plots). D_E varied from 25 to 28 m in the sheltered regions to 50 to 55 m in the exposed regions. SST gradients reach 2–3°C difference between sheltered and exposed regions around Santa Catalina Island. See color version of this figure at back of this issue.

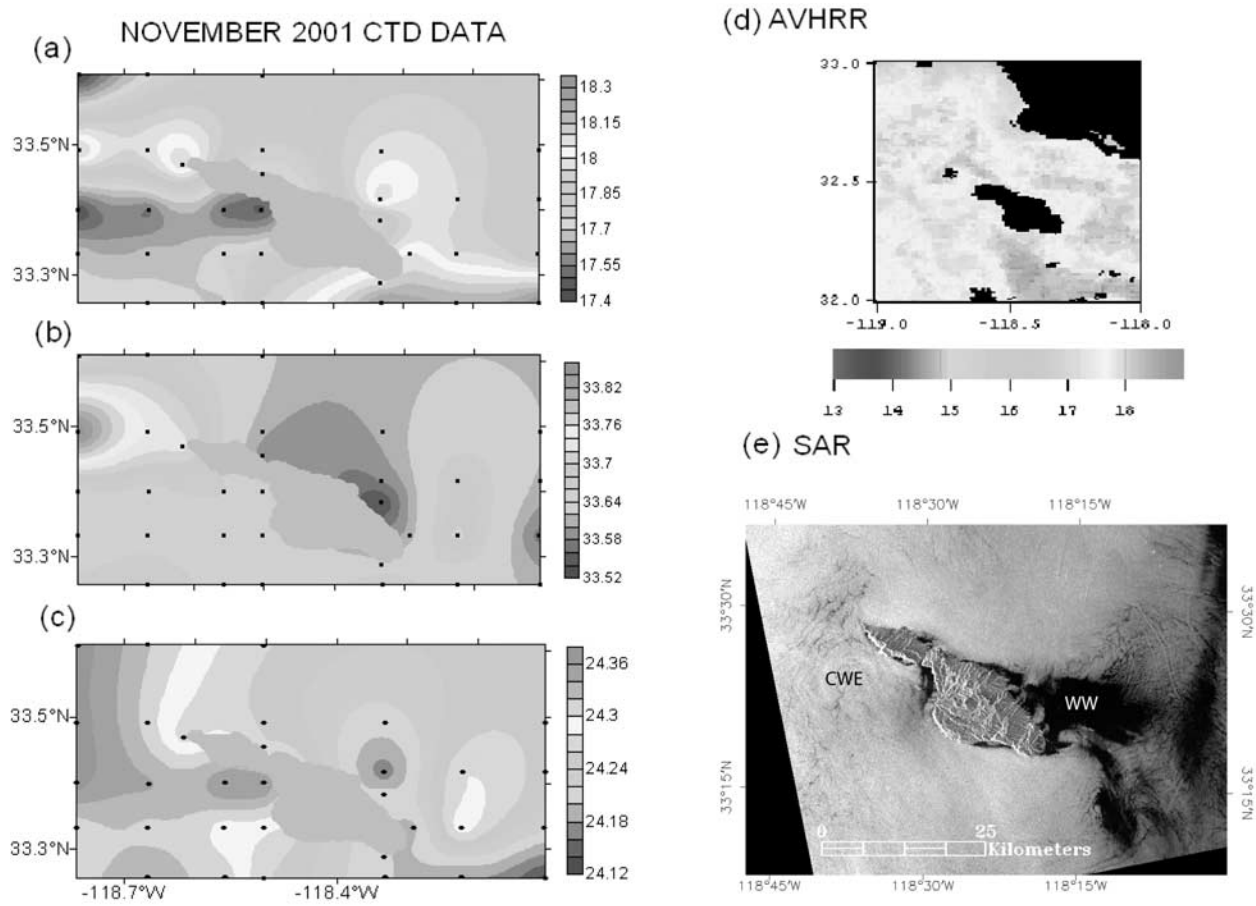

Figure 6. Data for the 16–20 November 2001 cruise: (a) temperature (in °C), (b) salinity (in ppt), and (c) σ_t (in kg m^{-3}). The data show a tongue of cold water to the northwest side of the island. Salinity and density were higher to the north as well. (d) AVHRR (19 November 2001, 1038 UTC) and (e) RADARSAT SAR image from 16 November 2001 at 0142 UTC. Interesting features are evident to the northwest of Catalina, including surface slicks potentially indicative of an eddy or other surface circulation feature. The same area seen by AVHRR (Figure 6d) is somewhat colder (1°C) than its surroundings. Copyright Canadian Space Agency 2001. See color version of this figure at back of this issue.

to the formation of a wake, which exhibits wave disturbances or instabilities at its interface with the undisturbed current. Very high R_e ($80 < R_e < 90$) produce the separation of the vortices from the obstacle. Vortices separate in turn from either side and drift away with a velocity of $0.8U$, forming a downstream sequence of vortices with alternate sense of rotation, the so-called Von Karman Vortex Street [*Tomczak and Godfrey*, 1994]. Eddies are intense energy dissipaters and island current wakes are regions of high-energy dissipation. The R_e value derived to characterize the different wake types was done by towing an object through a tank with fluid at rest. In the ocean, however, the currents are moved by winds, internal pressure gradients, or tides. There are also important distinctions that should be made between island wakes in deep water and in shallow water [*Wolanski et al.*, 1984] (see also 1998 lecture notes by M. Tomczak, available at http://gyre.umeoce.maine.edu/physicalocean/Tomczak/ShelfCoast/index.html, hereinafter referred to as Tomczak lecture notes, 1998). However, given that our Ekman depth D_E is much less than the ocean surrounding water depth (H^2), Santa Catalina Island should induce deep ocean–type current wakes. Therefore, for an average speed of CCC of 0.3 m s^{-1} (CalCOFI data), considering an average value for A_h of 100 m^2 s^{-1} [*Aristegui et al.*, 1994] (see also Tomczak lecture notes, 1998), the R_e for Catalina is 58, which predicts a wake formation with wave disturbances but not as fully turbulent as a Von Karman Vortex Street (ROMS scenario c discussed below; see Figure 7c). Important to note however, is that Catalina Island shelf is not a cylinder such as the model

Figure 7. Snapshots from ROMS 1-year simulation showing the progressive (9-day) formation of a northwest island wake with the eddy advecting away from the island after 9 days. The eddy was anticyclonic and reached 30 km in diameter. The anticyclonic eddy left a cyclonic feature with convergence and cold water to the northwest of the island. This ROMS scenario is similar to the current island wake measured during the November 2001 cruise. Color bars represent SST anomalies. See color version of this figure at back of this issue.

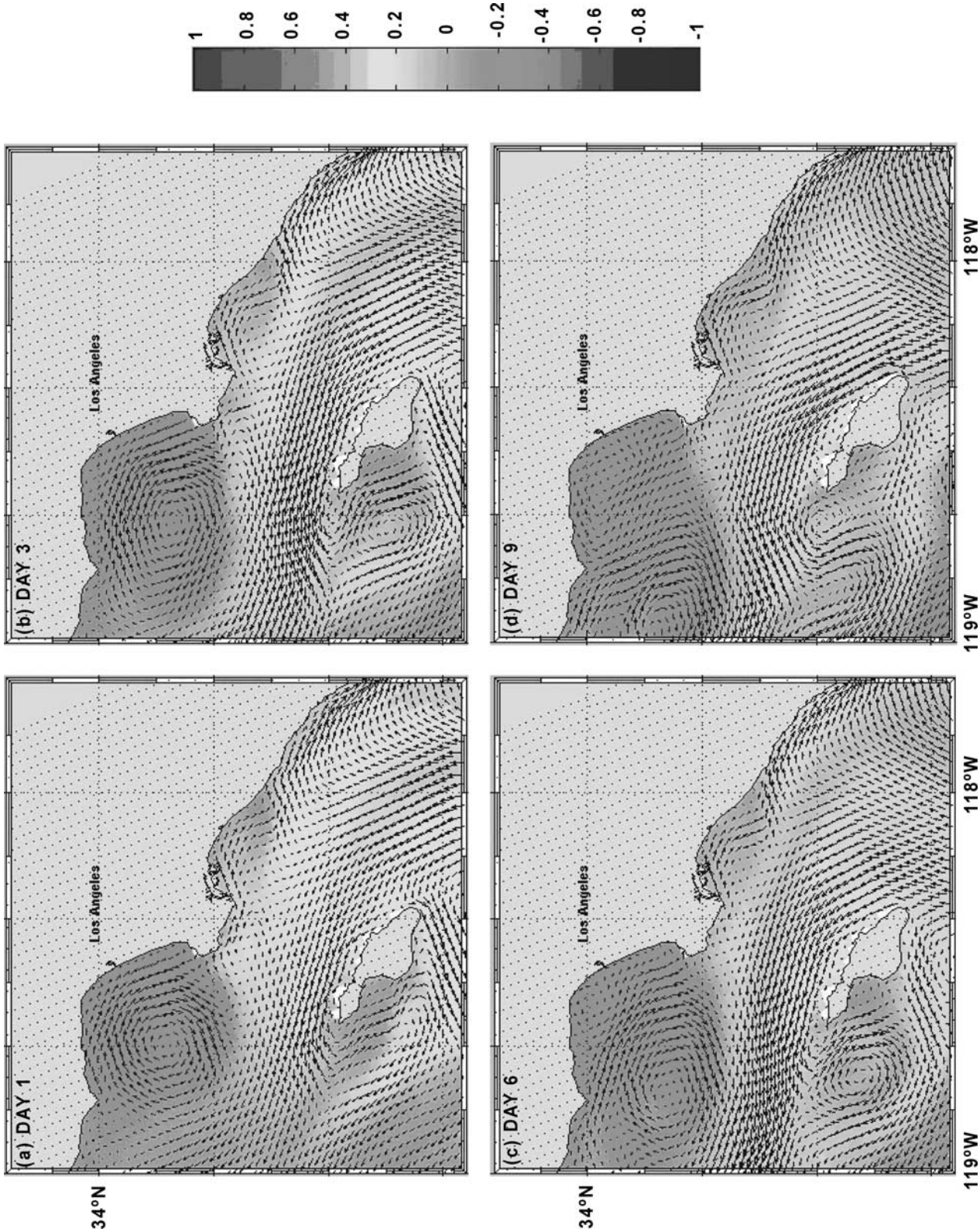
1
0.8
0.6
0.4
0.2
0
-0.2
-0.4
-0.6
-0.8
-1
(a) DAY 1
(b) DAY 3
(c) DAY 6
(d) DAY 9
Los Angeles
34°N
119°W
118°W

Figure 7

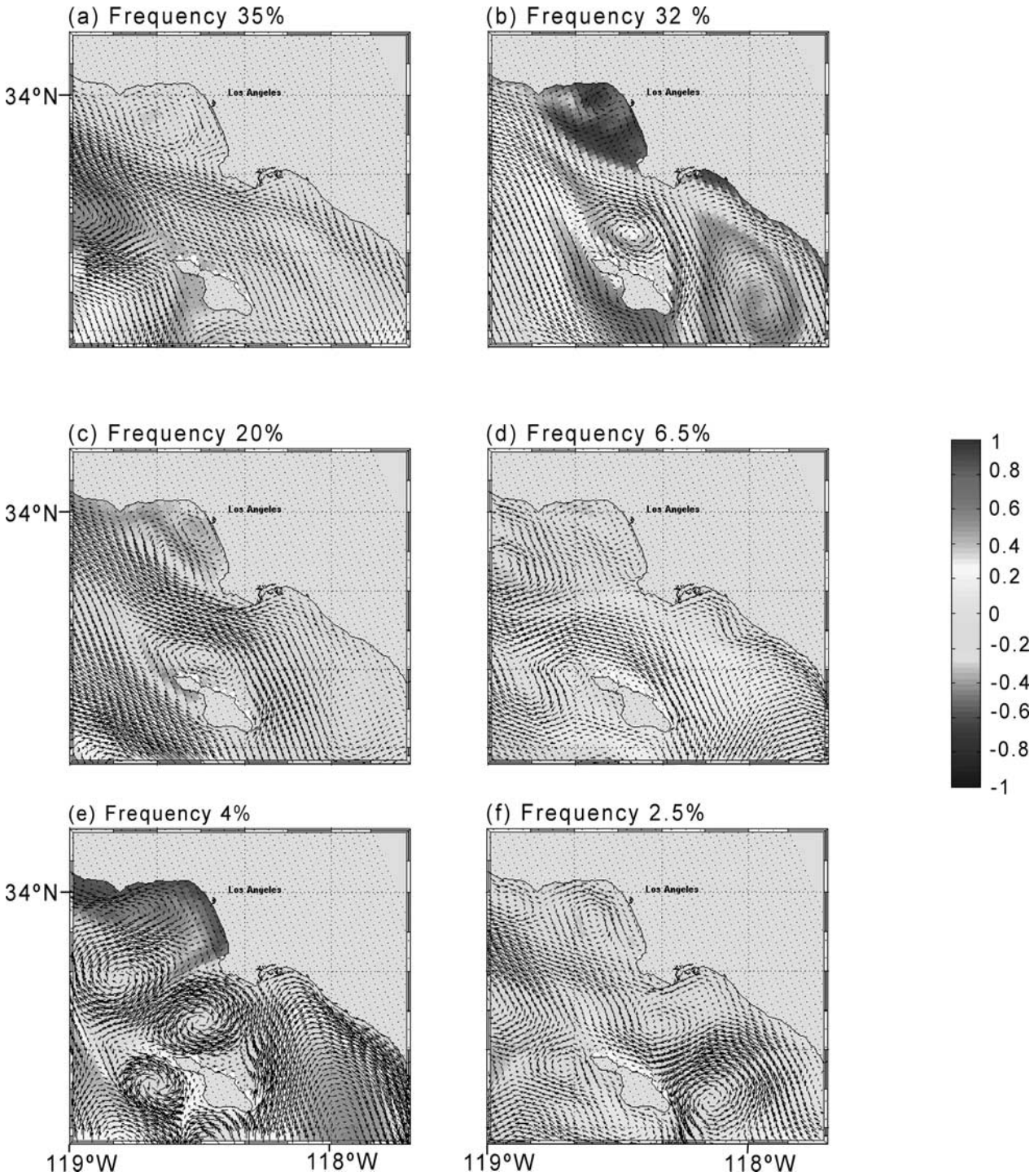

Figure 8. Current island wake scenarios resolved by ROMS during the 1-year simulation ordered from most abundant to less abundant: (a) west wake, (b) northeast eddy, (c) north Von Karman Street with upwelling of cold water, (d) northwest eddy, (e) dipole eddies to the north of the island, and (f) southeast eddy. Color bar represents SST anomalies. See color version of this figure at back of this issue.

islands used in laboratory simulations; it is ridge-like in shape and therefore a three-dimensional numerical model such as ROMS, would better represent the dynamics of the flow.

4.2.3. Numerical Simulation Study

[32] The formation of a northwest wake as observed during our November 2001 cruise is well illustrated by ROMS simulations (Figures 7a–7d). Four snapshots, 3 days apart, show an anticyclonic eddy being formed on the west side of Catalina Island (Figure 7a), requiring a total of 9 days from the birth to detachment (Figure 7d). The eddy reached 30 km in diameter and transported cold water in its core. The angle of the jet affecting Catalina at the time was normal to the island shelf. However, because of the asym-

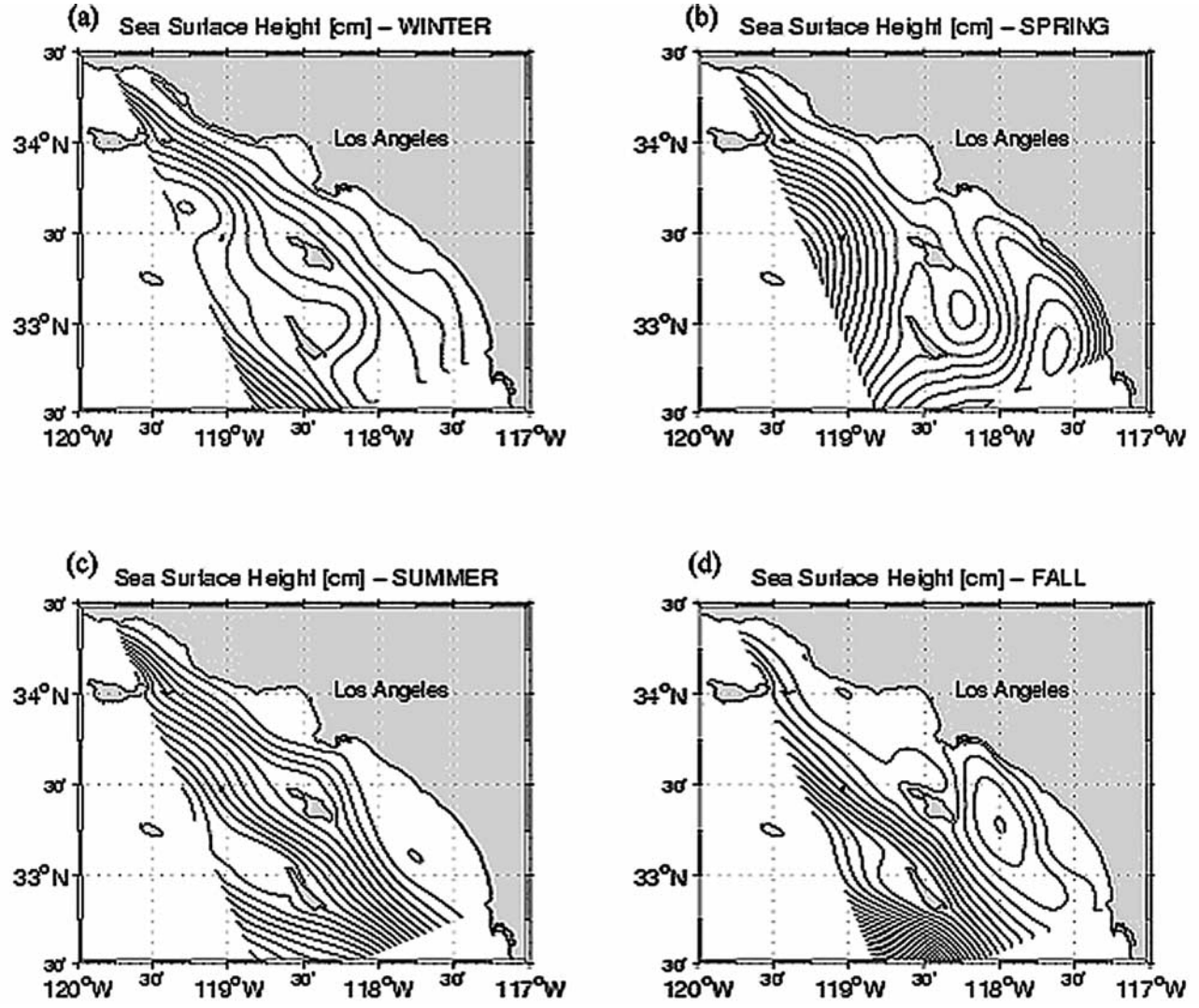

Figure 9. Sea surface height analysis for the Southern California Bight from level 3 (2 km) embedded domain. There is a wake signature even in the mean seasonal fields, and the strongest wakes occur in summer when the poleward California Countercurrent is also the strongest. Winter and summer showed wakes to the north of Catalina Island, whereas spring and fall have shown wakes to the south. These 3-year seasonal averages contain signatures of mesoscale features. Units are in centimeters, and the contour interval is 0.5 cm.

metric shape of the island, slightly bulging to the west, the island offers unequal resistance to the incoming current.

[33] To assess the occurrence of this and other wake scenarios we analyzed 1-year ROMS solutions, after the model reached equilibrium (Figure 8 and Animation 1). Six different scenarios were distinguished using ROMS solutions. The percentages indicate how often they occurred within the 121 yearly frames analyzed (every 3 days). The six patterns of flow are: (1) west island wake, 35%; (2) northeast eddy, 32%; (3) north Von Karman Street with upwelling of cold water, 20%; (4) northwest eddy, 6.5%; (5) dipole eddies to the northwest and northeast of the island, 4%; and (6) southeast eddy, 2.5%.

[34] There were also various combinations of these six scenarios. For example, the northwest wake scenario often evolved into Von Karman Streets and/or northwest eddies. After a brief period of time (9–12 days), fully formed eddies spun from the north side of the island. Another example of the complexity of flow regimes is illustrated by Figure 8f. This snapshot shows a cyclonic eddy forming to the southeast of the island; however, there are also anticyclonic and cyclonic eddies forming to the northeast and to the west of the island. We do not contend with these examples that we have fully evaluated the dynamics of the surface ocean currents around Santa Catalina Island. We do wish to illustrate, however, that a classical approach which averages long-term geostrophic conditions will not take into consideration all the island wakes scenarios compiled herein (Figure 8).

[35] Eddies that spun off the shelf of Catalina Island in ROMS simulation often reached Santa Monica Bay (SMB) and other coastal areas. Conversely, eddies being formed within the SMB sometimes reached the Channel Islands. Because of the complex nature of the surface currents in this

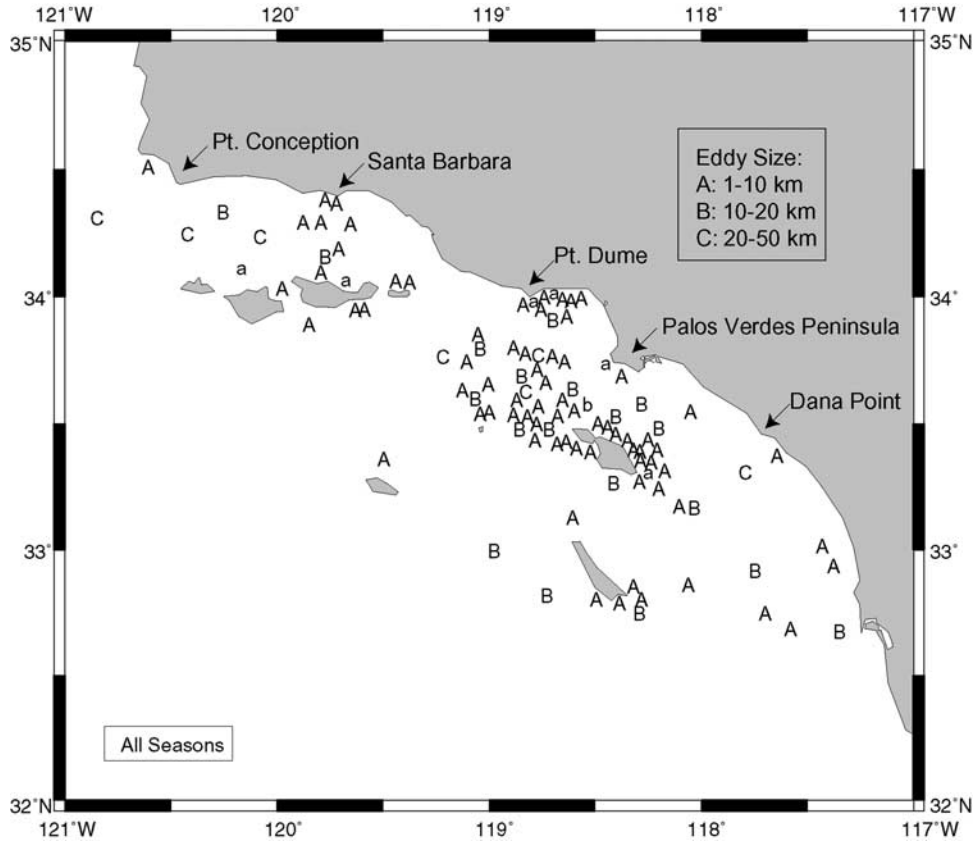

Figure 10. Total distribution map of eddies detected in the Southern California Bight via ERS-1 and ERS-2 SAR images from 1992 to 1998. Size of eddies is indicated as follows: A, 1–10 km; B, 10–20 km; C, 20–50 km and greater. Capital letters indicate cyclonic eddies, and lowercase letters indicate anticyclonic eddies [*DiGiacomo and Holt*, 2001].

region, we suggest that equatorial flow might also occur in other periods around Catalina Island. *Bray et al.* [1999], for example, suggested that the equatorial flow in the Bight might be a result of coastal upwelling. However, equatorward traveling geostrophic eddies (30–60 km), as shown in our simulations, also cause an equatorward transport at the surface, between Palos Verdes and Catalina Island.

[36] The simulations also highlight geostrophically balanced flow, off southern California, divided by the Santa Rosa Ridge; with poleward flow within the Bight and equatorward flow offshore. The exception occurs in spring when the equatorward anomaly weakens or reverses the poleward flow in the Bight (as previously emphasized by *Hickey* [1992, 1993, 1998]). In contrast, in our numerical solutions for flow on each side of Catalina Island, opposing flows were often observed. For example, San Pedro Basin regularly exhibited surface flows travelling in the opposite direction to flows in the Catalina Basin, between San Clemente and Catalina (also shown by drifter data discussed below).

[37] ROMS simulations suggest that a small change in the angle of attack of the incoming current can dramatically change the nature of the island current wakes. For example, scenario b in Figure 8 was induced by a strong jet reaching the island, at a 45° angle from the west, whereas scenario a was induced by the convergence of opposing currents to the west of Santa Catalina.

[38] The resident time of eddies and wakes, formed around islands are of great importance when considering their biological effects [*Hamner and Hauri*, 1981a, 1981b; *Wolanski and Hamner*, 1988; *Wolanski et al.*, 1984]. Eddies and wakes might function as retention belts for eggs and larvae [*Caldeira et al.*, 2001]. Plankton communities around Santa Catalina Island's shelf are significantly different from plankton communities away from shore, in deeper oceanic waters (R. Caldeira et al., Island-induced (meso)zooplankton communities: a case study around Santa Catalina Island, Southern California Bight, manuscript in preparation, 2005).

[39] In terms of the temporal variability in ROMS simulations we found that current wakes are often formed to the north of Santa Catalina during winter and summer (Figures 9a and 9c) and to the south/southeast during spring and fall (Figures 9b and 9d). Figure 9 shows contours of sea surface height (SSH) derived from the ROMS solutions discussed above. Each plot represents the average conditions for a season. Sea Surface Height is a good measurement of the island wake activity since island generated eddies, fronts and upwelling systems promote convergent and divergent circulation cells with a SSH signature. We present ROMS SSH scenarios as probable seasonal average conditions for the SCB; as suggested by *Bray et al.* [1999] there are local and remote wind–forcing circulation patterns in the SCB which can only be resolved with a wind-driven model for the whole region. The one-way nesting procedure

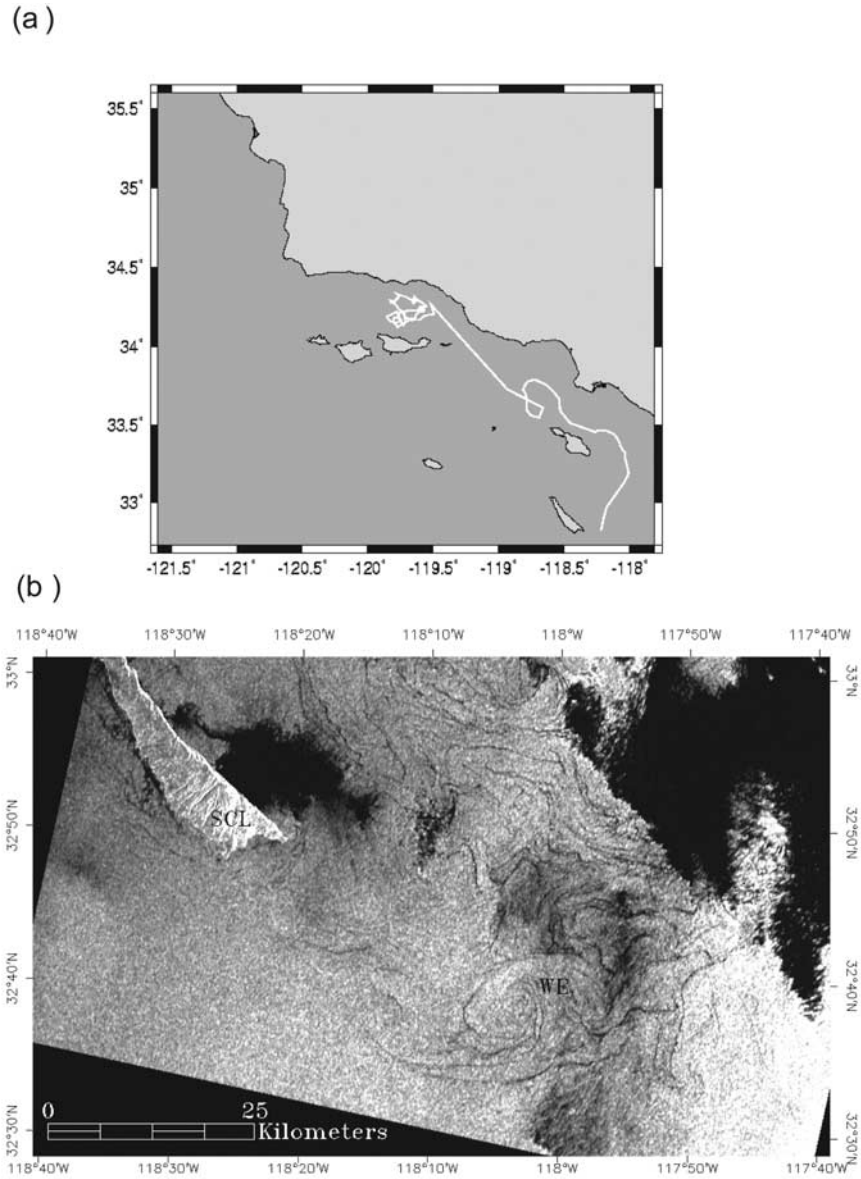

Figure 11. (a) Track of drifter 256 from a January 1996 drifter release as part of the Santa Barbara Channel–Santa Maria Basin Coastal Circulation Study [*Winant et al.*, 1999]. This drifter was released in the Santa Barbara Channel, north of Santa Cruz Island. (b) ERS-2 SAR image of San Clemente Island and vicinity on 27 January 1996 at 1832 UTC. Area WE denotes wake eddy, and SCL denotes San Clemente Island. Copyright ESA 1996.

used (adaptive grid refinement in FORTRAN (AGRIF)) extensively described by *Blayo and Debreu* [1999] enabled for an increase in eddy kinetic energy resolved in the child model (2.2 km) which became crucial in resolving the detailed island wake activity around Santa Catalina Island. Further details of the embedded method used in ROMS will be discussed elsewhere. The north (winter and summer) (Figures 9a and 9c) and south (spring and fall) (Figures 9b and 9d) current wake patterns reflect well the seasonality of the wind stress patterns in the SCB. *Bray et al.* [1999] showed that poleward flow in the SCB is maximum in the winter and summer and that there is an equatorial anomaly in the alongshore current associated with a wind stress during spring.

4.2.4. Submesoscale Dynamics in the SCB

[40] Some of the interesting submesocale dynamics that take place around Santa Catalina Island were described recently by *DiGiacomo and Holt* [2001]. On the basis of SAR imagery acquired between 1992 to 1998, approximately half of the SCB submesoscale eddy activity they observed occurred around Santa Catalina Island (Figure 10). However, the majority of these (~66%) were submesoscale eddies of 1–10 km diameter, whereas in our ROMS solutions the diameter of most eddies varied between 10 and 30 km. There

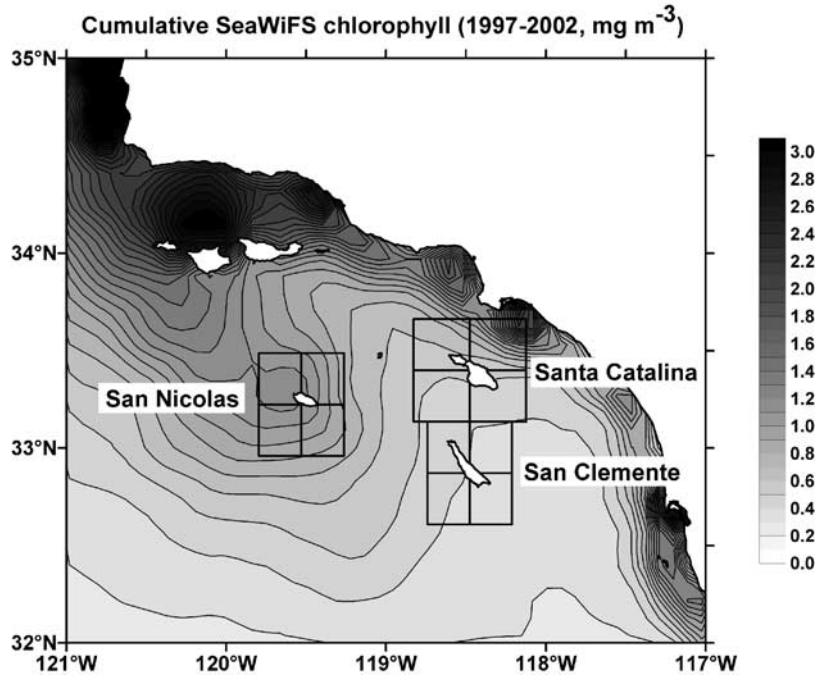

Figure 12. Cumulative distribution of surface chlorophyll in the Southern California Bight averaged over the entire period of SeaWiFS observations (September 1997 to July 2002). The rectangles around three islands (San Nicolas, San Clemente, and Santa Catalina) indicate the zones where level 3 data pixels were averaged for time series analysis.

are also more anticyclonic features in the ROMS solutions than were observed by the SAR imagery. These differences are potentially attributable to a number of factors. First, the resolution of the SAR imagery (~100 m) is significantly greater than that of ROMS solutions (2 km). Also, observations of larger eddies may be effectively limited by the size of the ERS-1/2 SAR images (100 × 100 km), potentially skewing the relative abundance toward smaller size classes. Regarding the relative distribution of cyclonic versus anticyclonic eddies, the submesoscale eddies observed in the SAR study were primarily of the "spiral" variety as described by *Munk et al.* [2000]. This latter study indicated that surfactants might preferentially concentrate within cyclonic convergence zones, thereby potentially allowing spiral eddies to be visualized more readily (e.g., in SAR images) than anticyclonic eddies. However, the authors also noted that cyclonic rotation in spiral eddies is favored for numerous reasons: (1) shear, (2) static, (3) centrifugal, and (4) inertial instabilities, which can limit anticyclonic development. In this context, the physical properties of an eddy, for example, size, rotational sense, vertical structure and surface signatures (e.g., via temperature or roughness), can vary depending upon the type or class of eddy being observed. As eddies are generated through a variety of mechanisms in the SCB, future studies should work toward distinguishing between the types of eddies observed in model output and satellite imagery in order to better understand their properties and potential impacts.

[41] The SCB region, because of its bathymetric configuration is obviously very complex and island-induced wakes are frequent. These cannot be resolved from long-term average data. Eddies in our simulations and observations are short lived around Catalina Island (3–7 days). Because of their frequent occurrences they must have important effects in overall poleward and equatorward transport in the San Pedro Basin, with implications for nutrient flux, productivity, plankton patchiness, larval transport and retention and dispersal of pollutants [*DiGiacomo and Holt*, 2001]. Seasonally, these authors found, most eddy activity around Catalina occurred during winter. Winter is also a seasonal maximum for the Southern California Countercurrent [*Hickey*, 1992, 1998]. Therefore strong poleward transport may frequently foster the formation of small-scale eddies around headlands and islands in the SCB.

4.3. Wakes Off Other Islands in the Southern California Bight

4.3.1. Wind Wakes

[42] Wind and current wakes are not unique to Santa Catalina Island but occur off most islands of the SCB. In fact, we hypothesize that current wakes contribute to a significant part of the submesoscale dynamics of the Bight and therefore to the input of nutrients to the euphotic zone. All islands of the Southern California Bight produce some manner of wind wakes as illustrated above (Figure 3d). On this occasion the Santa Rosa Island (SR) wind wake, reaches Santa Barbara Island (SB); the Santa Cruz Island (SCZ) wind wake reaches Santa Monica Bay (SMB); the San Nicholas (SN) wind wake runs 50 km south, approximately eight times the diameter of the island; the Santa Catalina Island and San Clemente Island (SCL) wind wakes can be distinguished also. We have identified numerous ERS-1/2 and RADARSAT SAR images that show concurrent incidences of wind wakes off multiple SCB islands. As such, SCB island wind wake effects should not necessarily

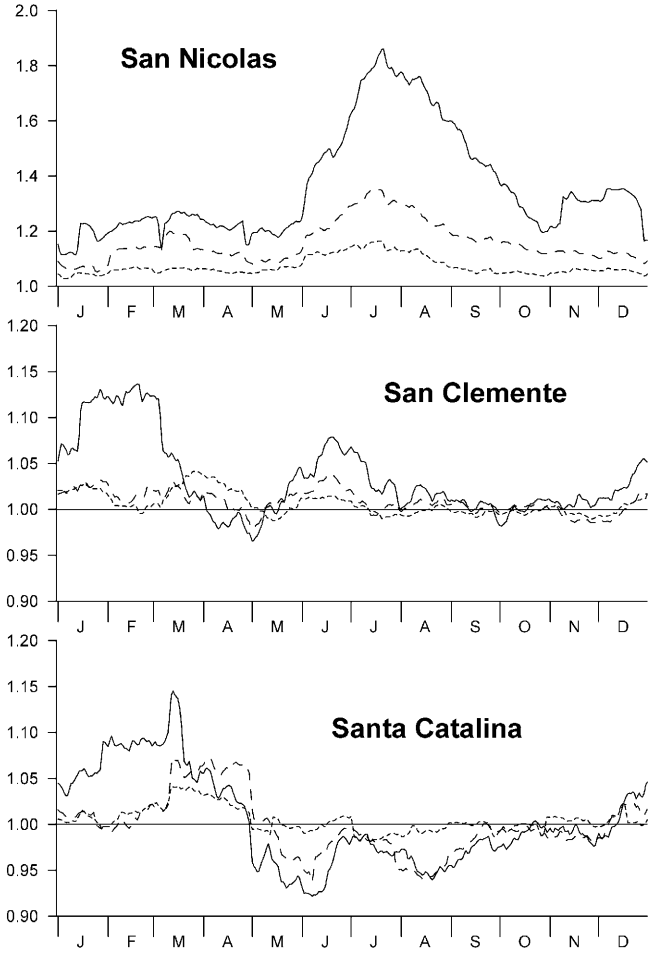

Figure 13. "Island mass effect" of San Nicholas, San Clemente, and Santa Catalina islands on productivity. Shown are seasonal variations of the ratios between SeaWiFS chlorophyll medians in the rectangles 2 × 2 and 8 × 8 (solid line), 4 × 4 and 8 × 8 (dashed line), and 6 × 6 and 8 × 8 (dotted line).

be considered independently in future surveys. For example, the Santa Rosa wind wake shown above (Figure 3d) apparently reaches as far as Santa Catalina Island and impacts the local sheltering effects of that island. Another aspect that was clear from our review of these SAR images was that offshore islands, although smaller, showed longer leeward streets as a result of stronger offshore winds. According to *Bray et al.* [1999], wind stress curl is stronger (4 μPa/m) between the channel islands and Point Conception all year round when compared to the rest of the Bight (<1 μPa/m). As shown by *Bray et al.* [1999, Plate 6], the highest stress curl occurs between Santa Rosa and Santa Catalina, sometimes reaching San Clemente Island (highest for spring and summer). Therefore future studies might also want to consider the relative contribution of each island to the overall sheltering effect of the inshore waters.

4.3.2. Current Wake Off San Clemente Island

[43] ERS-1/2 SAR imagery (during the two missions so-called "tandem phase") from 26 January (not shown) and 27 January (Figure 11b), 1996, revealed a current eddy southeast of San Clemente Island that was approximately 18 km in diameter. It had an apparent translational speed of 9 cm s^{-1} and it tracked east-southeast over the course of 2 days. Near-coincident drifter releases from the Santa Barbara Channel–Santa Maria Basin Coastal Circulation Study [*Winant et al.*, 1999] revealed that flow during this time was indeed equatorward (Figure 11a), supporting the above interpretation of the equatorward forcing of this eddy. These San Clemente wake eddies are often observed in our extensive ERS-1/2 and RADARSAT SAR archive and deserve further investigation.

4.4. Time Series Analysis and the "Island Mass Effect Phenomenon"

[44] The cumulative remotely sensed surface chlorophyll concentration for the Southern California Bight (Figure 12) reflects the climatology of both productivity and hydrology of the region. The highest concentration was detected near the continental shelf (~3 mg m^{-3}) and at the upwelling region of Point Conception (PC), compared to the (1–1.5 mg m^{-3}) around the islands. However, time series variability around Santa Catalina, San Clemente and San Nicholas islands (square regions in the cumulative distribution map of Figure 12), shows a seasonal pattern around the islands (Figure 13). This suggested the occurrence of nutrient enrichment around islands and the occurrence of the "island mass effect."

[45] The effect of San Nicolas Island on surface chlorophyll concentration is most pronounced, especially during summer months (Figure 13). In July and August the chlorophyll concentration in the small quadrants is almost twice the background concentration. This effect is also present in the map of cumulative chlorophyll distribution in the Southern California Bight (Figure 12). The island mass effect of San Clemente and Santa Catalina islands is not as evident (Figure 13). In late winter and early spring (January–March) chlorophyll concentration in the small quadrants exceeds the background concentration by 10–15%. Later no significant differences were observed. During late spring and summer (especially in May and August) Santa Catalina Island shows a "negative island mass effect." By negative island mass effect we mean that the background chlorophyll concentration exceeds the values observed in the small quadrants.

[46] We believe that the negative island mass effect around Santa Catalina results from its proximity to shore, under the influence of the coastal high chlorophyll concentrations; the northern eastern part of the 8 × 10 rectangle is located within the continental shelf zone, where chlorophyll concentration is always higher than offshore. In general however, the seasonality of the island mass effect for Santa Catalina and San Clemente Islands could be related to the seasonality of the California Countercurrent. *Hickey* [1998] showed that poleward flow within the Bight is strongest during winter and summer months. Therefore we would expect that current wakes and subsequent upwelling of cold nutrient rich waters to be highest during such events; this is also in agreement with our averaged SSH from ROMS numerical solutions.

[47] Looking at the individual island cases increase in sea surface chlorophyll is often concurrent with decrease in SST (Figures 14a–14c). For San Nicholas, we hypothesize

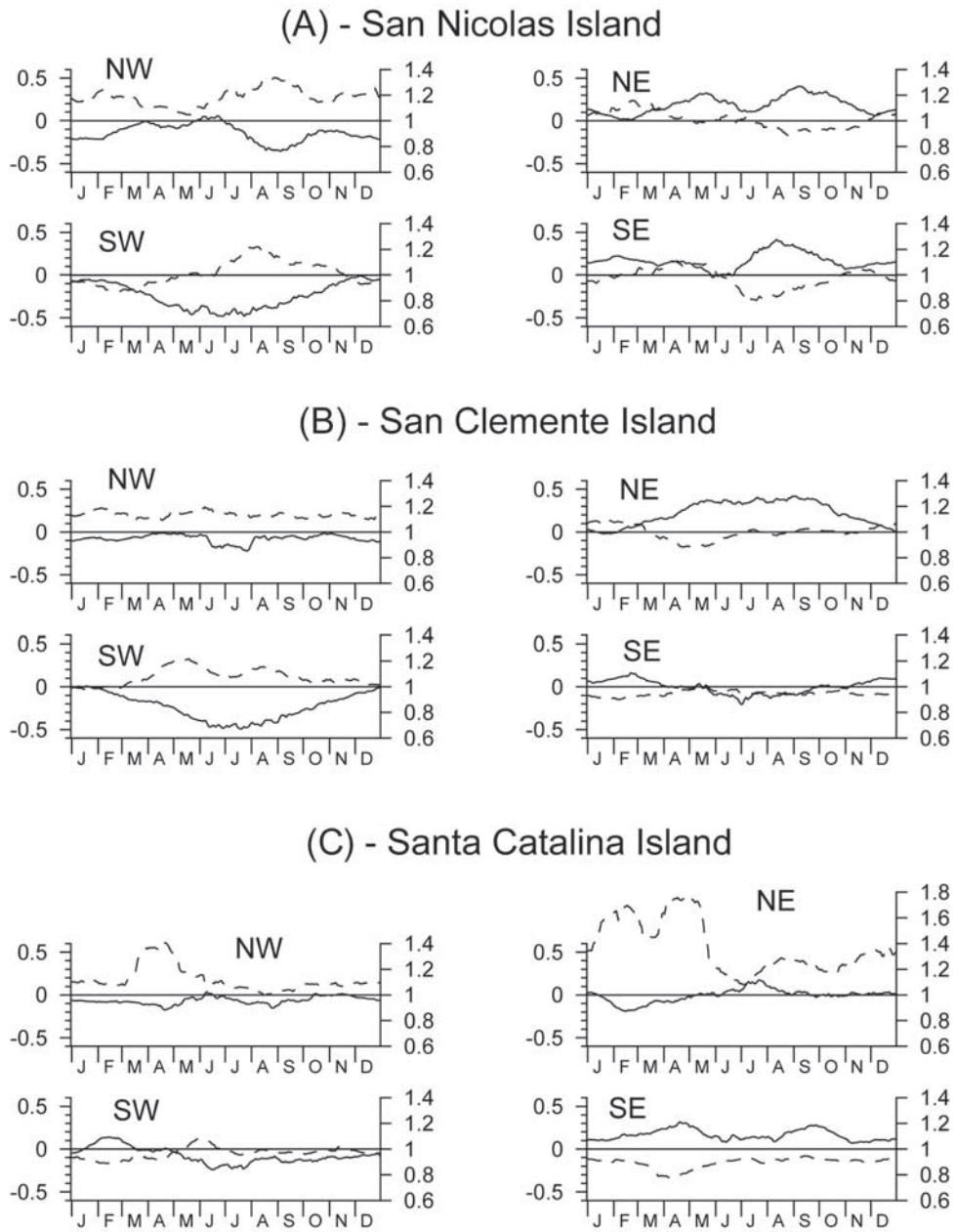

Figure 14. Difference between sea surface temperature and derived chlorophyll, in 3 × 3 quadrants located in four directions around the islands and 6 × 6 background values surrounding the islands: (a) San Nicholas Island, (b) San Clemente Island, and (c) Santa Catalina Island. Data show decrease in SST (solid line) concurrent with increase in sea surface chlorophyll (dashed line).

that the summer increase in chlorophyll concentration is related to the inshore shift and increase in the equatorial flow often observed for the California Current [*Bray et al.*, 1999].

[48] Figures 14a–14c illustrate the SST anomalies in 3 × 3 quadrants located to NW, NE, SW, and SE of each island (here we use the term "anomalies" meaning the differences between SST in the 3 × 3 quadrant and the background SST in 6 × 6 quadrant surrounding the entire island).

[49] The remote-sensed surface chlorophyll concentration to the NW of San Nicolas Island is permanently higher (Figure 14a); it results from general gradient of chlorophyll concentration in SCB (see Figure 12). California Current transports cold rich in chlorophyll water from NW along San Nicolas Island. At the same time, chlorophyll heterogeneity directed to the NE, SW, and SE of San Nicholas exhibits seasonal variations. In late winter (February–March) positive chlorophyll gradient is directed to the NE, then (April–May) it shifts to the SE, and later (starting from July) it is directed to the SW, when the equatorward effect of the CC is supposedly greater [*Bray et al.*, 1999]. The regularities of spatial heterogeneity of chlorophyll resulting from seasonal variations of circulation pattern are also evident on San Clemente Island (Figure 14b). To the NW of the island chlorophyll concentration is permanently higher. In winter chlorophyll is higher to the NE

whereas in summer and autumn it is higher to the SW of the island. San Clemente Island is located closer to the shore than San Nicholas. In summer, the strengthening of the California Countercurrent, which transports low chlorophyll water poleward, enhances the cross-shelf chlorophyll gradient. Chlorophyll distribution around Santa Catalina Island (Figure 14c) manifests two features: high chlorophyll concentration to the NE during winter-spring, and to the NW during spring. Higher chlorophyll concentrations to the NW of Santa Catalina Island in spring can be explained by CC migrating onshore,weakening of the CCC.

5. Conclusions

[50] Several conclusions can be drawn for this first study of island wakes in the SCB:

[51] Wind-induced island wakes must be distinguished from current-induced wakes. Santa Catalina Island, given that the predominant ocean currents flow opposite to the predominant wind conditions, offers a unique opportunity to explore the relative contribution of the two types of wakes on the transport and retention of biogenic materials. The central mountain range on Catalina Island offers resistance to the predominant incoming northeast winds, sheltering the leeward side of the island. Weaker wind in the lee induces weaker mixing and surface waters store more heat from the incident solar radiation [*Caldeira and Marchesiello*, 2002; *Robinson*, 1997]. The California Countercurrent moving poleward is disrupted by the bathymetry of the island, with formation of a current island wake to the north side of Catalina. Current and wind wakes occur on opposite sides of the island because of differences in the direction of the predominant wind and surface currents. This is the first time such features have been reported for opposite sides of an island. Most surface currents are wind driven and therefore wind and current directions are mostly parallel. Wind and current wakes around Catalina may also occur concurrently, particularly during strong equatorial push and/or Santa Ana wind events.

[52] Prior discussions on the mesoscale phenomena of the SCB have overlooked the importance of island wakes [*Bray et al.*, 1999; *Hickey*, 1979, 1991, 1992, 1993, 1998]. Wind and current wakes are also generated by other islands of the SCB and their relative importance and interaction require further attention. Future work should consider the use of integrated multisensor (e.g., ocean color, SAR, SST) approaches, using single (e.g., ENVISAT) or multiple platforms, to identify small-scale island-generated features in the SCB and elsewhere.

[53] Time series analysis suggests that there is a concurrence of low SST with increase in sea surface chlorophyll around Santa Catalina, San Clement and San Nicholas island mass effect. The seasonality of such events suggests that they might be related to the seasonality of the CC and CCC. Further studies should use numerical simulations in conjunction with in situ data to determine the forcing mechanisms that modulate the seasonality of the CC and CCC and determine their effect in the formation of island wakes in the SCB.

[54] **Acknowledgments.** We wish to acknowledge William Hamner and Peggy Fong for their editorial comments to early versions of the manuscript. We also wish to thank Renee Maabadi for helping with the processing of CTD data. We thank Ben Holt for assisting with the SAR data acquisition and interpretation and Clint Winant for supplying the Santa Barbara Channel drifter data. The JPL effort was supported by the National Aeronautics and Space Administration through a contract with the Jet Propulsion Laboratory, California Institute of Technology. R. M. A. Caldeira was supported by a Ph.D. scholarship from the Madeira Education Secretariat (POPRAM II/III). We are also greatly indebted to anonymous reviewers for their suggestions.

References

Acker, J., S. Shen, G. Leptoukh, G. Serafino, G. Feldman, and C. McClain (2002), SeaWiFS ocean color data archive and distribution system: Assessment of system performance, *IEEE Trans. Geosci. Remote Sens.*, *40*(1), 90–103.

Aristegui, J., P. Sangra, S. Hernadez-Leon, M. Canton, A. Hernandez-Guerra, and J. Kerling (1994), Island-induced eddies in the Canary Islands, *Deep Sea Res., Part I*, *41*, 1509–1525.

Aristegui, J., et al. (1997), The influence of island-generated eddies on chlorophyll distribution: A study of mesoscale variation around Gran Canaria, *Deep Sea Res., Part I*, *44*, 71–96.

Barkley, R. (1972), Johnston Atoll's wake, *J. Mar. Res.*, *30*(2), 201–216.

Barton, E., et al. (1998), The transition zone of the Canary Current upwelling region, *Prog. Oceanogr.*, *41*, 455–504.

Barton, E., G. Basterretxea, P. Flament, E. Mitchelson-Jacob, B. Jone, J. Aristegui, and F. Herrera (2000), Lee region of Gran Canaria, *J. Geophys. Res.*, *105*(C7), 17,173–17,193.

Blayo, E., and L. Debreu (1999), Adaptive mesh refinement for finite-difference ocean models: First experiments, *J. Phys. Oceanogr.*, *29*, 1239–1250.

Bray, N. A., A. Keyes, and W. M. L. Morawitz (1999), The California Current system in the Southern California Bight and the Santa Barbara Channel, *J. Geophys. Res.*, *104*(C4), 7695–7714.

Caldeira, R., and P. Marchesiello (2002), Ocean response to wind sheltering in the Southern California Bight, *Geophys. Res. Lett.*, *29*(13), 1635, doi:10.1029/2001GL014563.

Caldeira, R. M. A., P. Russell, and A. Amorim (2001), Evidence of an unproductive coastal front in Baia D'Abra, an embayment on the south east of Madeira Island, Portugal, *Bull. Mar. Sci.*, *69*(3), 1057–1072.

Caldeira, R. M. A., S. Groom, P. Miller, D. Pilgrim, and N. P. Nezlin (2002), Sea-surface signatures of the island mass effect phenomena around Madeira Island, Northeast Atlantic, *Remote Sens. Environ.*, *80*(2), 336–360.

Chavez, F. P. (1995), A comparison of ship and satellite chlorophyll from California and Peru, *J. Geophys. Res.*, *100*(C12), 24,855–24,862.

Clemente-Colon, P., and X. H. Yan (2000), Low backscatter ocean features in synthetic aperture radar imagery, *John Hopkins APL Tech. Dig.*, *21*(1), 116–121.

Coutis, P., and J. Middleton (1999), Flow-topography interaction in the vicinity of an isolated, deep ocean island, *Deep Sea Res., Part I*, *46*, 1633–1652.

Dietrich, D., M. Bowman, C. Lin, and A. Mestas-Nunez (1996), Numerical studies of small island wakes, *Geophys. Astrophys. Fluid Dyn.*, *83*, 195–231.

DiGiacomo, P. M., and B. Holt (2001), Satellite observations of small coastal ocean eddies in the Southern California Bight, *J. Geophys. Res.*, *106*(C10), 22,521–22,544.

DiGiacomo, P. M., L. Washburn, B. Holt, and B. Jones (2004), Coastal pollution hazards in southern California observed by SAR imagery: Stormwater plumes, wastewater plumes, and natural hydrocarbon seeps, *Mar. Pollut. Bull.*, *49*(11–12), 1013–1024.

Doty, L., and M. Oguri (1956), The island mass effect, *J. Cons. Cons. Perman. Int. Explor. Mer*, *22*, 33–37.

Furukawa, K., and E. Wolanski (1998), Shallow-water frictional effects in island wakes, *Estuarine Coastal Shelf Sci.*, *46*(4), 599–608.

Hamner, W., and I. Hauri (1981a), Effects of island mass: Water flow and plankton pattern around a reef in the Great Barrier Reef lagoon, Australia, *Limnol. Oceanogr.*, *26*(6), 1084–1102.

Hamner, W., and I. Hauri (1981b), Long-distance horizontal migrations of zooplankton (Scyphomedusae: Mastigias), *Limnol. Oceanogr.*, *26*(3), 414–423.

Haney, R., R. Hale, and D. Dietrich (2001), Offshore propagation of eddy kinetic energy in the California Current, *J. Geophys. Res.*, *106*(C6), 11,709–11,717.

Hernandez-Leon, S. (1988), Gradients of mesozooplankton biomass and ETS activity in the wind-shear area as evidence of an island mass effect in the Canary Island waters, *J. Plankton Res.*, *10*(6), 1141–1154.

Hernandez-Leon, S. (1991), Accumulation of mesozooplankton in a wake area as a causative mechanism of the "island-mass effect," *Mar. Biol.*, *109*, 141–147.

Hickey, B. M. (1979), The California Current system—Hypotheses and facts, *Prog. Oceanogr.*, *8*, 191–279.
Hickey, B. M. (1991), Variability in two deep coastal basins (Santa Monica and San Pedro) off southern California, *J. Geophys. Res.*, *96*(C9), 16,689–16,708.
Hickey, B. M. (1992), Circulation over the Santa Monica-San Pedro basin and shelf, *Prog. Oceanogr.*, *30*, 37–115.
Hickey, B. M. (1993), Physical oceanography, in *Ecology of the Southern California Bight*, edited by M. D. Dailey, D. Reish, and J. Anderson, pp. 19–70, Univ. of Calif. Press, Berkeley.
Hickey, B. M. (1998), Coastal oceanography of Western North America from the tip of Baja California to Vancouver Island, in *The Sea*, vol. 11, edited by A. R. Robinson and K. H. Brink, pp. 345–393, John Wiley, Hoboken, N. J.
Imberger, J. (1985), The diurnal mixed layer, *Limnol. Oceanogr.*, *30*(4), 737–770.
Joint Panel on Oceanographic Tables and Standards (1991), Processing of oceanographic station data, report, U. N. Educ., Sci., and Cult. Org., Paris.
Lynn, R., and J. Simpson (1987), The California Current System: The seasonal variability of its physical characteristics, *J. Geophys. Res.*, *92*(C12), 12,947–12,966.
Marchesiello, P., J. McWilliams, and A. Shchepetkin (2001), Open boundary conditions for long-term integration of regional oceanic models, in *Ocean Modell. 3*, pp. 1–20, Hooke Inst. Oxford Univ., Oxford, U. K.
Marchesiello, P., J. C. McWilliams, and A. Shchepetkin (2003), Equilibrium structure and dynamics of the California Current System, *J. Phys. Oceanogr.*, *33*, 753–783.
McClain, E., W. Pichel, and C. Walton (1985), Comparative performance of AVHRR-based multichannel sea surface temperatures, *J. Geophys. Res.*, *90*(C6), 11,587–11,601.
Munk, W., K. L. Armi, F. Fischer, and A. Zachariasen (2000), Spirals on the sea, *Proc. R. Soc. London, Ser. A*, *456*, 1217–1280.
Owen, R. W. (1980), Eddies of the California current system: Physical and ecological characteristics, in *The California Islands: Proceedings of a Multidisciplinary Symposium*, edited by D. M. Power, pp. 237–263, Santa Barbara Mus. of Nat. Hist., Santa Barbara, Calif.
Penven, P., L. Debreu, P. Marchesiello, and J. C. McWilliams (2003), Application of the ROMS embedding procedure in the California Current System, in *Ocean Modell.*, Hooke Inst. Oxford Univ., Oxford, U. K., in press.
Reid, J., and A. W. Mantyla (1976), The effect of the geostrophic flow upon coastal sea elevations in the northern North Pacific Ocean, *J. Geophys. Res.*, *81*, 31,000–31,010.
Rissik, D., I. M. Suthers, and C. T. Taggart (1997), Enhanced particle abundance in the lee of an isolated reef in the south Coral Sea: The role of flow disturbance, *J. Plankton Res.*, *19*(9), 1347–1368.
Robinson, I. S. (1997), *Satellite Oceanography: An Introduction for Oceanographers and Remote Sensing Scientists*, John Wiley, Hoboken, N. J.
Shchepetkin, A., and J. McWilliams (1998), Quasi-monotone advection schemes based on explicit locally adaptive dissipation, *Mon. Weather Rev.*, *126*, 1541–1580.
Shchepetkin, A. F., and J. C. McWilliams (2003), A method for computing horizontal presure-gradient force in an ocean model with a nonaligned vertical coordinate, *J. Geophys. Res.*, *108*(C3), 3090, doi:10.1029/2001JC001047.
Shchepetkin, A. F., and J. C. McWilliams (2005), The regional oceanic modeling system (ROMS): A split-explicit, free-surface, topography-following-coordinate oceanic model, in *Ocean Modell.*, Hooke Inst. Oxford Univ., Oxford, U. K., in press.
Smith, R. C., and K. Baker (1978), The bio-optical state of ocean waters and remote sensing, *Limnol. Oceanogr.*, *23*(2), 247–259.
Sverdrup, H., and R. Fleming (1941), The waters off the coast of southern California, March to July 1937, *Bull. Scripps Inst. Oceanogr. Tech. Ser.*, *4*, 261–378.
Tomczak, M., and J. Godfrey (1994), *Regional Oceanography: An Introduction*, Elsevier, New York.
Walton, C. (1988), Non-linear multichannel algorithms for estimating sea surface temperature with AVHRR satellite data, *J. Appl. Meteorol.*, *27*, 115–124.
Winant, C. D., D. J. Alden, E. P. Dever, K. A. Edwards, and M. C. Hendershott (1999), Near-surface trajectories off central and southern California, *J. Geophys. Res.*, *104*(C7), 15,713–15,726.
Wolanski, E., and W. Hamner (1988), Topographically controlled fronts in the ocean and their biological influence, *Science*, *241*, 177–181.
Wolanski, E., J. Imberger, and M. Heron (1984), Island wakes in shallow coastal waters, *J. Geophys. Res.*, *89*(C6), 10,553–10,569.
Wolanski, E., T. Asaeda, A. Tanaka, and E. Deleersnijder (1996), Three-dimensional island wakes in the field, laboratory experiments and numerical models, *Cont. Shelf Res.*, *16*, 1437–1452.

R. M. A. Caldeira, Center for Macaronesian Studies, University of Madeira, Campus da Penteada, 9000-390 Funchal, Madeira Island, Portugal. (rui.caldeira@uma.pt)
P. M. DiGiacomo, Jet Propulsion Laboratory, California Institute of Technology, MS 300-323, 4800 Oak Grove Drive, Pasadena, CA 91109-8099, USA.
P. Marchesiello and J. C. McWilliams, IGPP, University of California, 405 Hilgard Avenue, Los Angeles, CA 90095-1567, USA.
N. P. Nezlin, Southern California Coastal Water Research Project, 7171 Fenwick Lane, Westminster, CA 92683-5218, USA.

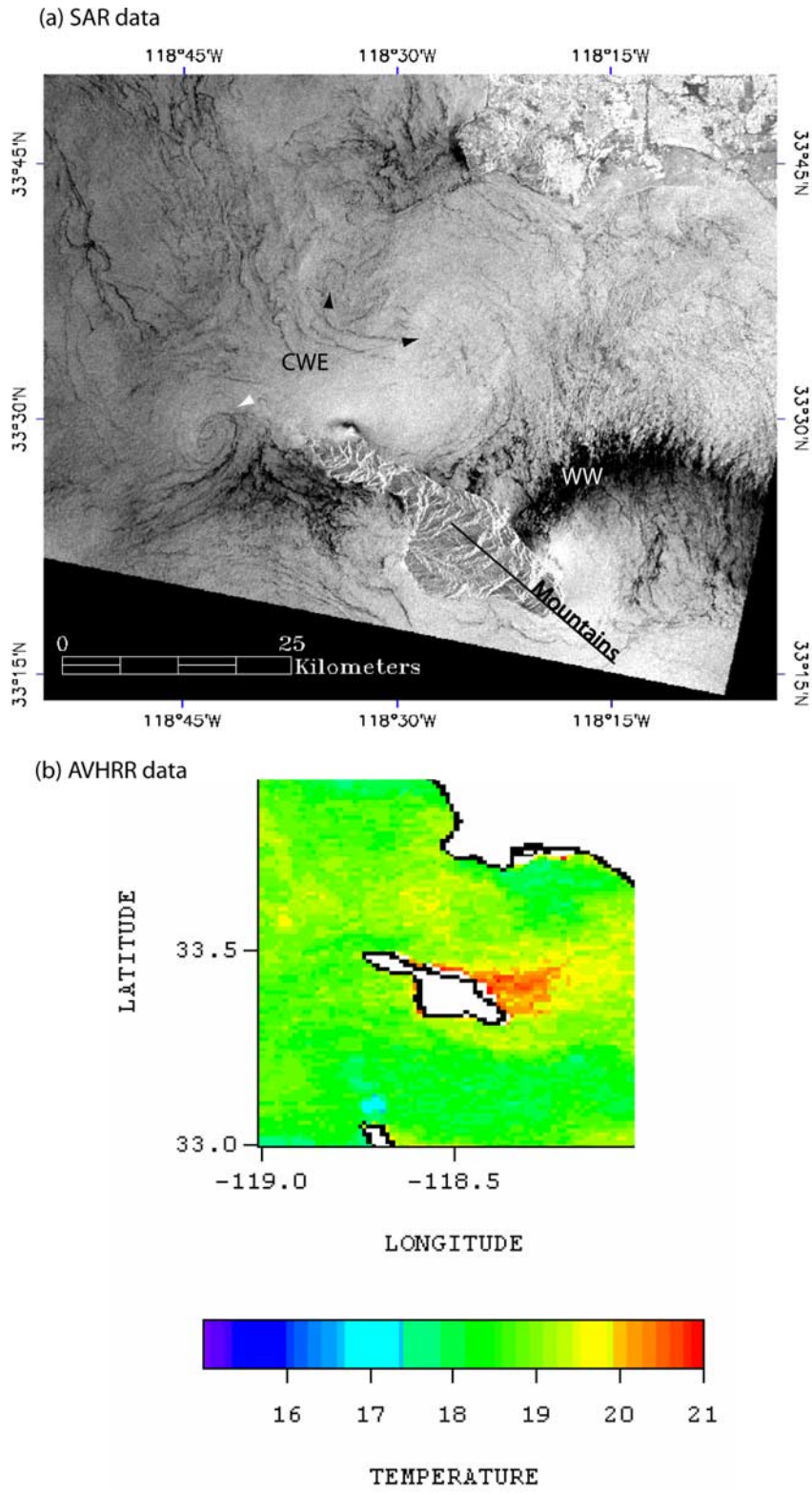

Figure 2. (a) ERS-1 synthetic aperture radar (SAR) image acquired 28 May 1994 at 1834 UTC. Spiral current wake eddies (~10 km in diameter) are visible off the northwest end of Santa Catalina Island (CWE), as is a wind wake (WW) off the island's eastern end. Other features are visible in the channel adjoining the mainland. Copyright ESA 1994. (b) AVHRR data collected on 29 May (0038 UTC). A warm wind–induced wake is visible in the lee of Catalina.

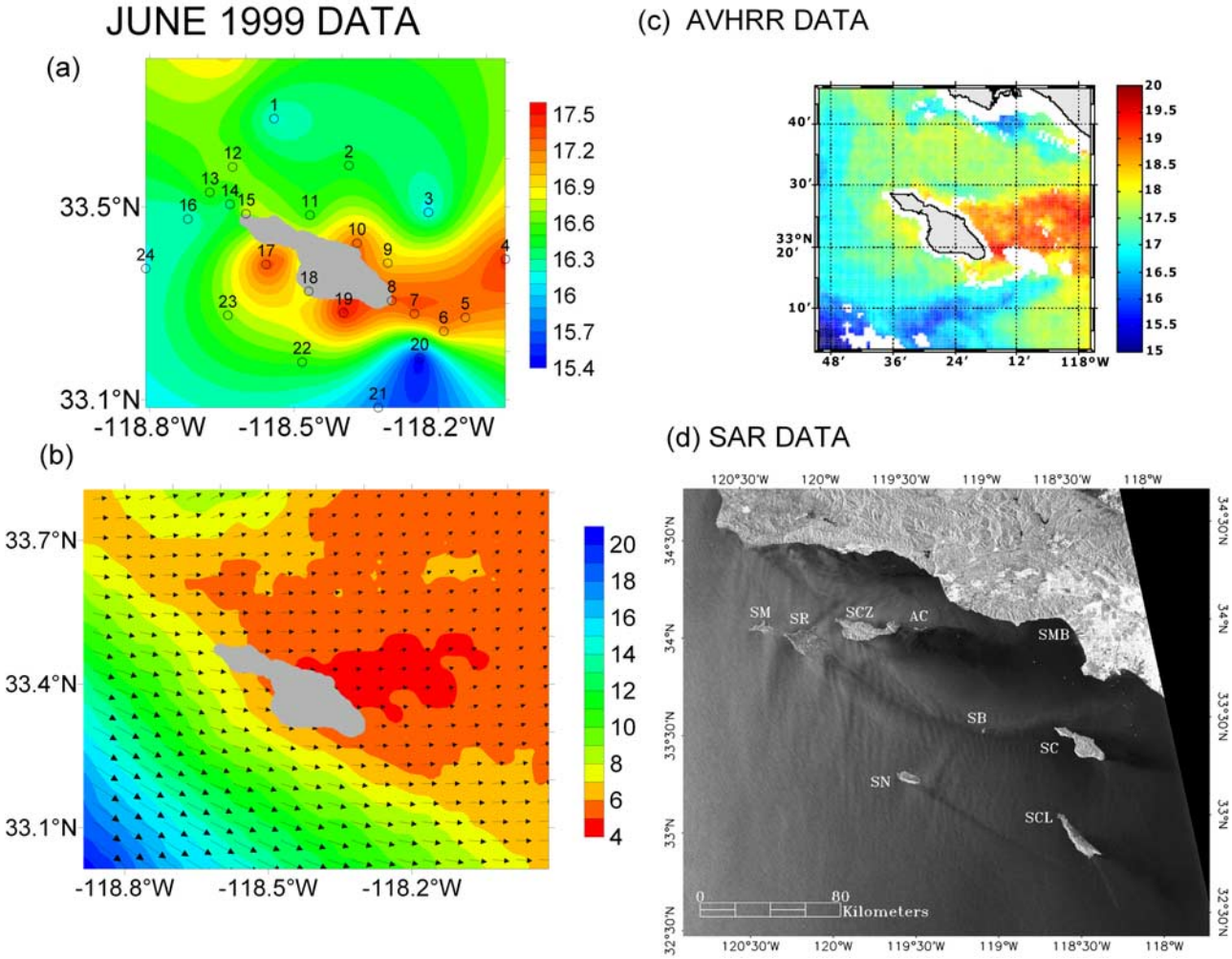

Figure 3. In situ data for June 1999: (a) temperature, (b) Ekman depths (D_E) and wind fields from COAMPS, (c) AVHRR data for the same period showing warmer SST leeward of Santa Catalina Island, and (d) RADARSAT ScanSAR image from 8 June 1999 at 0200 UTC of the entire Southern California Bight. Evident are the recurring wind wakes off the larger islands within the SCB. The Santa Rosa Island (SR) wind wake on this occasion appeared to reach all the way to Santa Catalina Island (SC). The Santa Cruz Island (SCZ) wind wake reached Santa Monica Bay (SMB). The San Nicholas (SN) wind wake runs (∼50 km) to the southeast. Santa Catalina and San Clemente Island (SCL) wind wakes were also clearly visible. SM denotes San Miguel Island; AC denotes Ana Capa Island; and SB denotes Santa Barbara Island. Copyright Canadian Space Agency 1999.

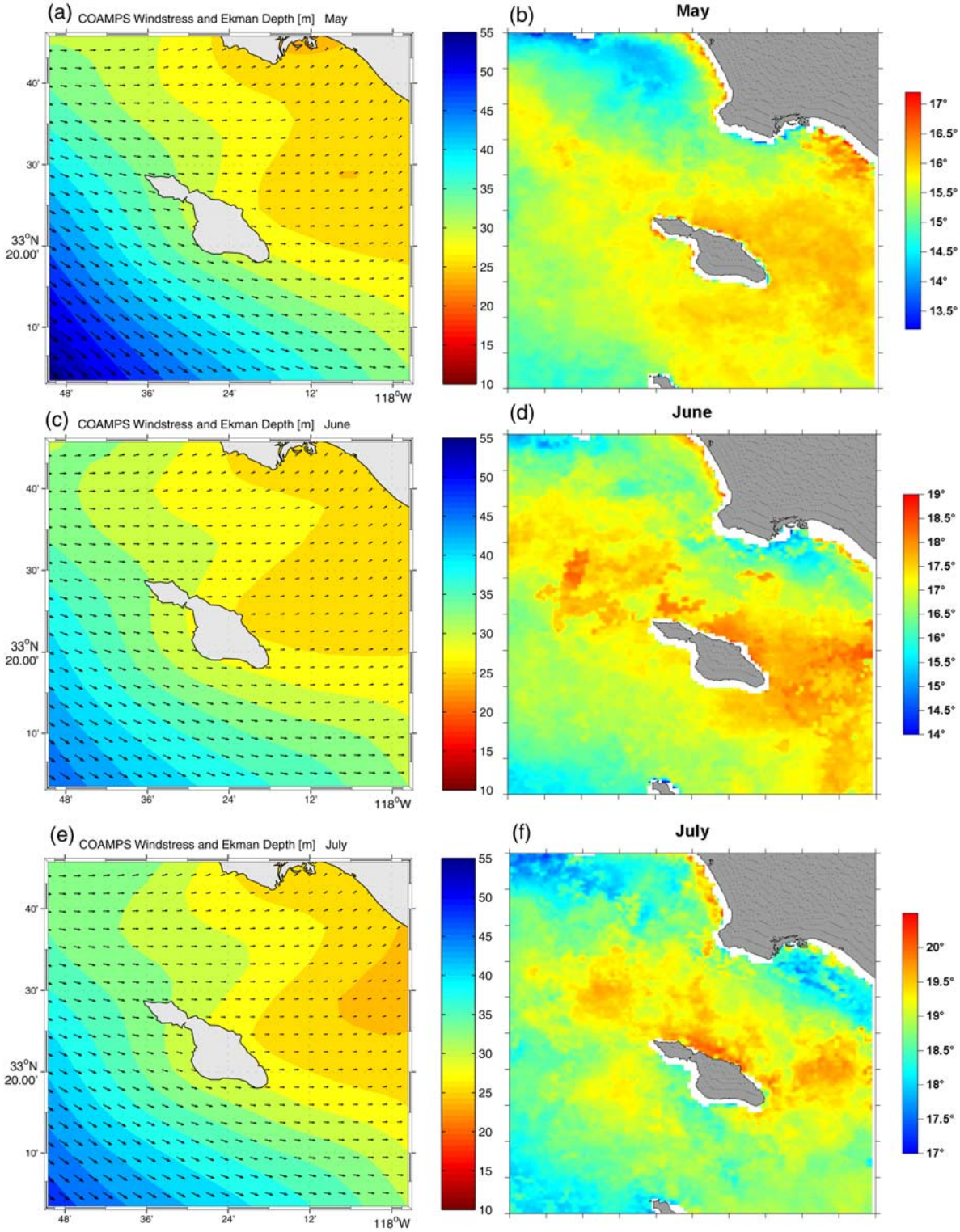

Figure 5. Average wind and SST conditions for the period of May to July (1998–2000 data). Left plots represent wind conditions and Ekman depths (D_E), color scale in meters, and right plots represent SST, color scale in degrees Celsius. As is evident, wind-sheltering effects off the southeast end of Santa Catalina occur most strongly during spring and summer. Winds are also generally stronger during spring and summer. Stronger winds caused stronger gradients on the Ekman depth, suggesting weaker wind mixing. Weaker mixing allows for higher heat storage and warmth of the SST leeward of the island (left plots). D_E varied from 25 to 28 m in the sheltered regions to 50 to 55 m in the exposed regions. SST gradients reach 2–3°C difference between sheltered and exposed regions around Santa Catalina Island.

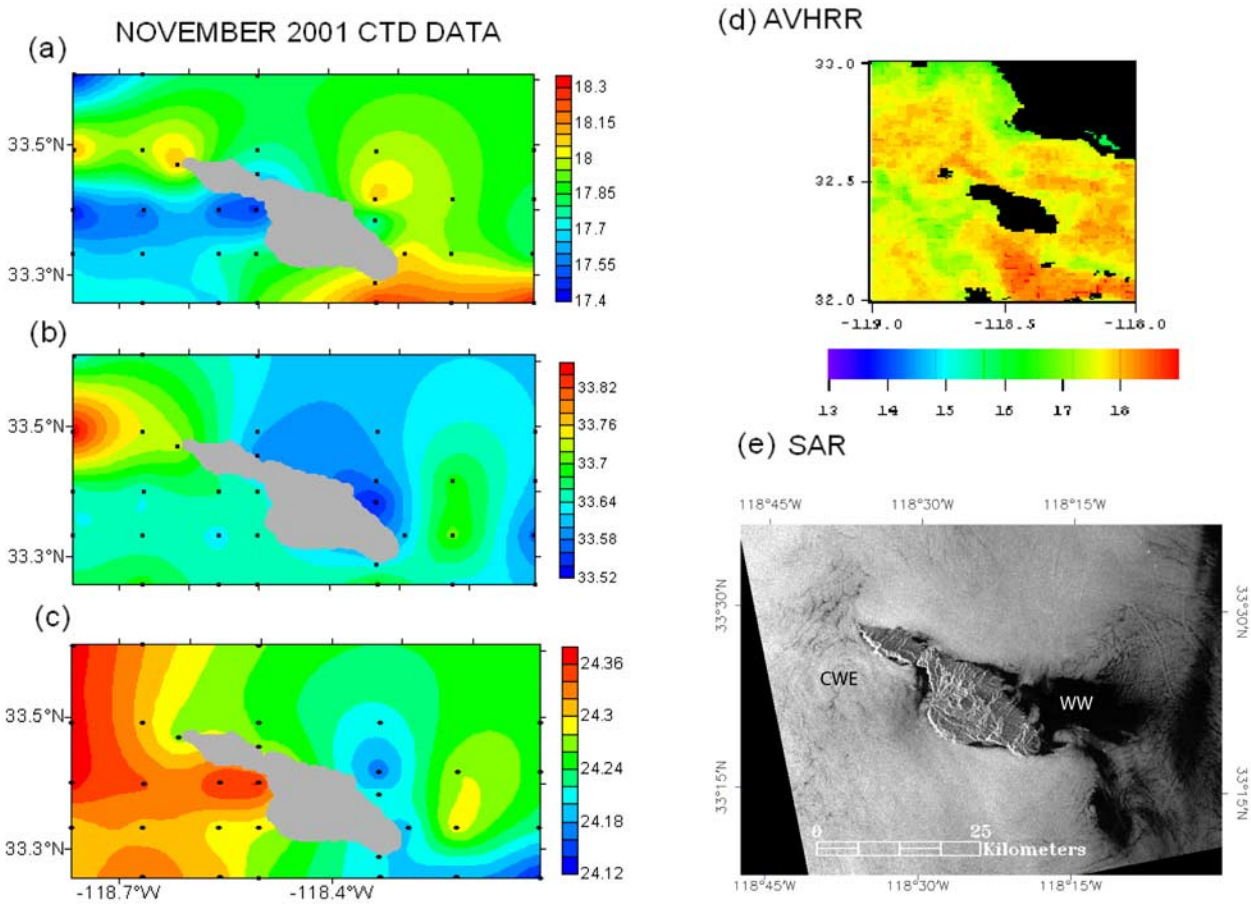

Figure 6. Data for the 16–20 November 2001 cruise: (a) temperature (in °C), (b) salinity (in ppt), and (c) σ_t (in kg m^{-3}). The data show a tongue of cold water to the northwest side of the island. Salinity and density were higher to the north as well. (d) AVHRR (19 November 2001, 1038 UTC) and (e) RADARSAT SAR image from 16 November 2001 at 0142 UTC. Interesting features are evident to the northwest of Catalina, including surface slicks potentially indicative of an eddy or other surface circulation feature. The same area seen by AVHRR (Figure 6d) is somewhat colder (1°C) than its surroundings. Copyright Canadian Space Agency 2001.

Figure 7. Snapshots from ROMS 1-year simulation showing the progressive (9-day) formation of a northwest island wake with the eddy advecting away from the island after 9 days. The eddy was anticyclonic and reached 30 km in diameter. The anticyclonic eddy left a cyclonic feature with convergence and cold water to the northwest of the island. This ROMS scenario is similar to the current island wake measured during the November 2001 cruise. Color bars represent SST anomalies.

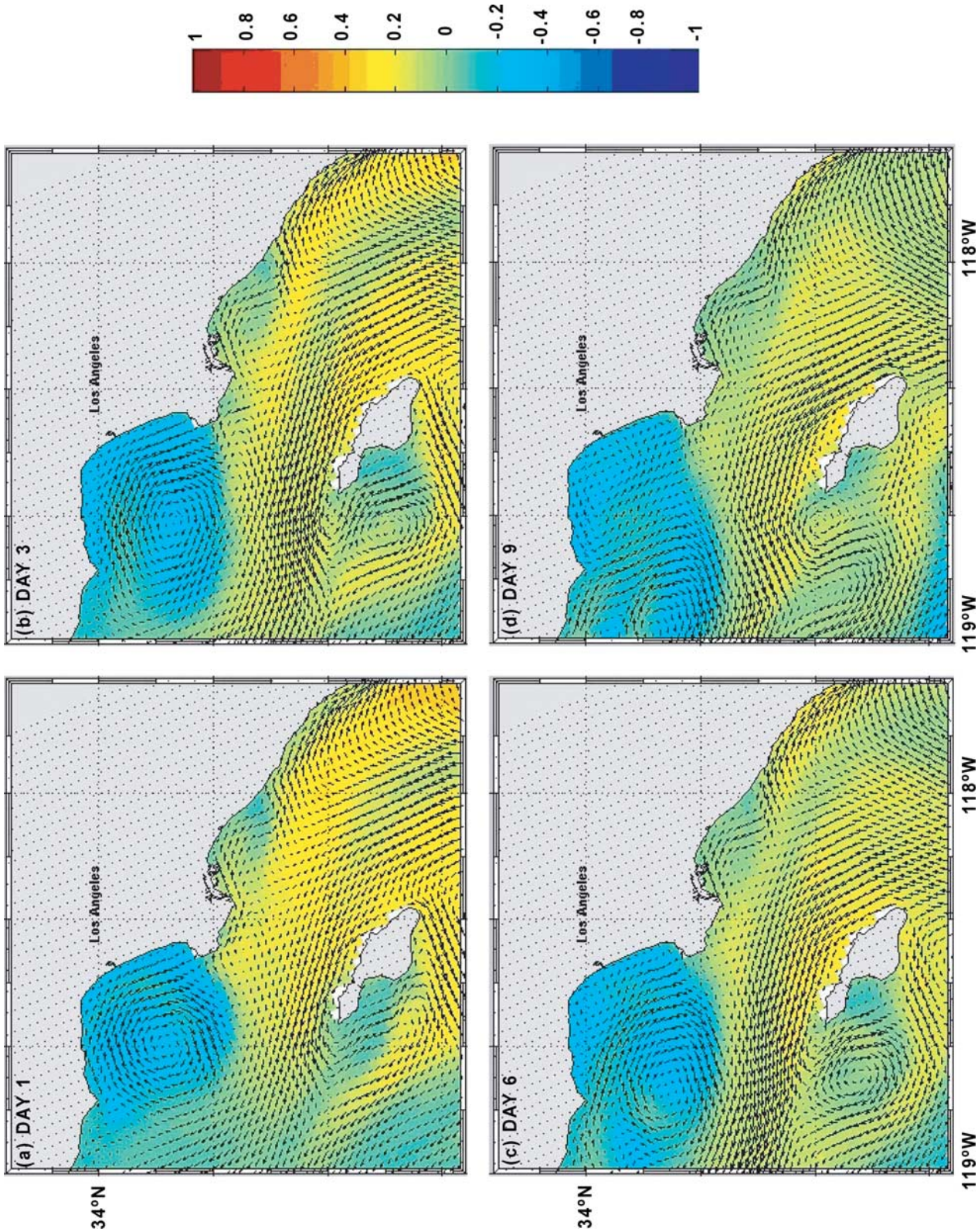
1
0.8
0.6
0.4
0.2
0
-0.2
-0.4
-0.6
-0.8
-1
(a) DAY 1
(b) DAY 3
(c) DAY 6
(d) DAY 9
Los Angeles
34°N
119°W
118°W

Figure 7

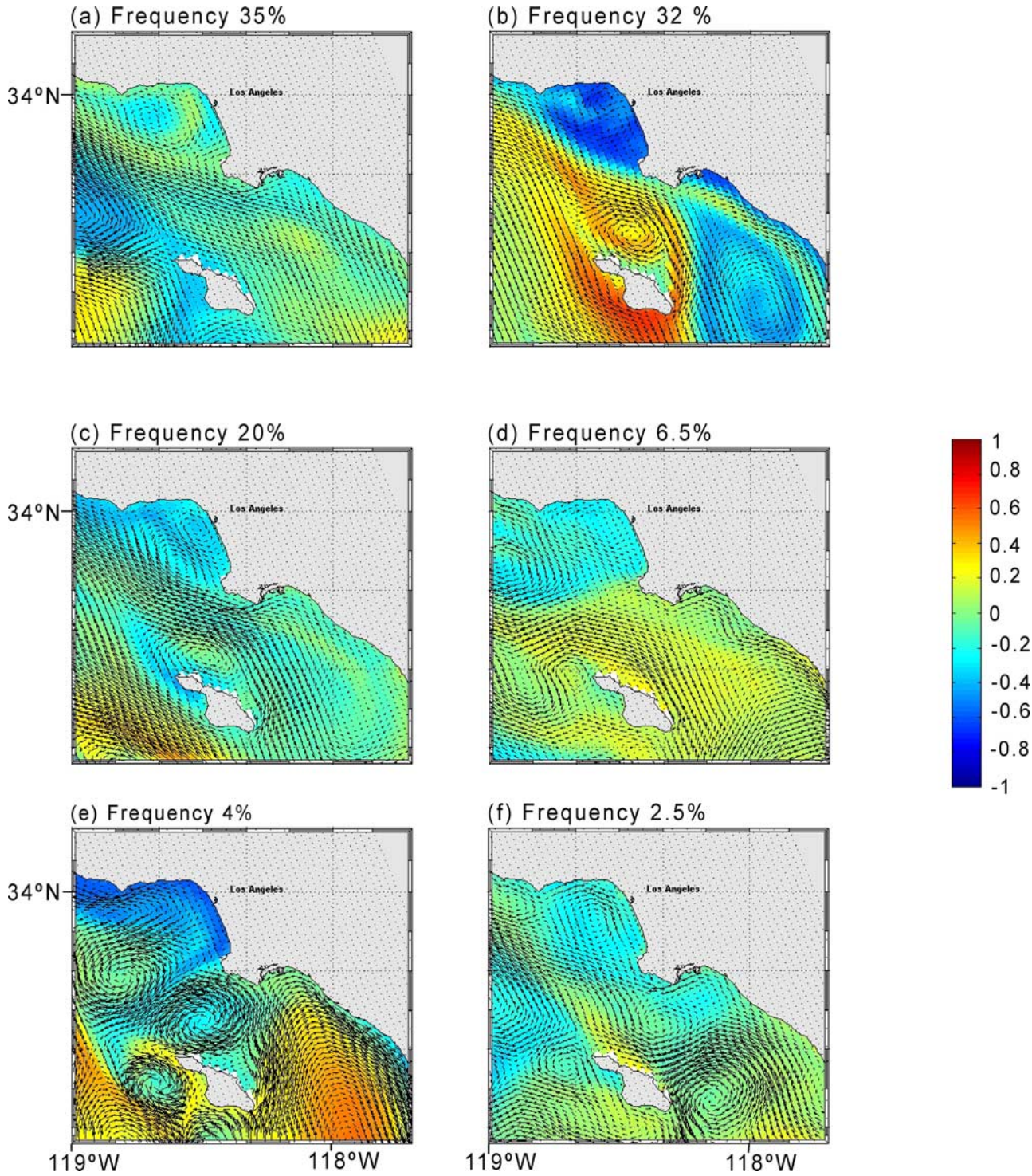

Figure 8. Current island wake scenarios resolved by ROMS during the 1-year simulation ordered from most abundant to less abundant: (a) west wake, (b) northeast eddy, (c) north Von Karman Street with upwelling of cold water, (d) northwest eddy, (e) dipole eddies to the north of the island, and (f) southeast eddy. Color bar represents SST anomalies.